

SEAMM: A Simulation Environment for Atomistic and Molecular Modeling

Paul Saxe,^{*,†,‡} Jessica Nash,^{*,†,‡} Mohammad Mostafanejad,^{*,†,‡} Eliseo
Marin-Rimoldi,^{*,¶} Hasnain Hafiz,^{*,§} Louis G Hector, Jr.,^{*,§} and T. Daniel
Crawford^{*,†,‡}

[†]*Department of Chemistry, Virginia Tech, Blacksburg, Virginia 24061, USA*

[‡]*Molecular Sciences Software Institute, Blacksburg, Virginia 24060, USA*

[¶]*Department of Chemical and Biomolecular Engineering, University of Notre Dame, Notre
Dame, Indiana 46556, USA*

[§]*Battery Research and Development, General Motors, Warren, MI 48092, USA*

E-mail: psaxe@vt.edu; janash@vt.edu; smostafanejad@vt.edu; emarinri@nd.edu;
hasnain.hafiz@gm.com; louis.hector@gm.com; crawdad@vt.edu

Abstract

The Simulation Environment for Atomistic and Molecular Modeling (SEAMM) is an open-source software package written in Python that provides a graphical interface for setting up, executing, and analyzing molecular and materials simulations. The graphical interface reduces the entry barrier for the use of new simulation tools, facilitating the interoperability of a wide range of simulation tools available to solve complex scientific and engineering problems in computational molecular science. Workflows are represented graphically by user-friendly flowcharts which are shareable and reproducible. When a flowchart is executed within the SEAMM environment, all results, as well as metadata describing the workflow and codes used, are saved in a datastore that can be

viewed using a browser-based dashboard, which allows collaborators to view the results and use the flowcharts to extend the results. SEAMM is a powerful productivity and collaboration tool that enables interoperability between simulation codes and ensures reproducibility and transparency in scientific research.

Keywords: Molecular dynamics simulation, electronic structure theory, density functional theory, molecular and materials modeling

Introduction

computational molecular science (CMS) and computational materials science (also CMS – we will use the term to encompass both) have been growing in importance since their beginning over 70 years ago. Figure 1 shows the growth of citations of the major CMS software packages in the international scientific literature as well as international patents, which are proxies for basic and applied research. Citation statistics for the CMS codes, obtained

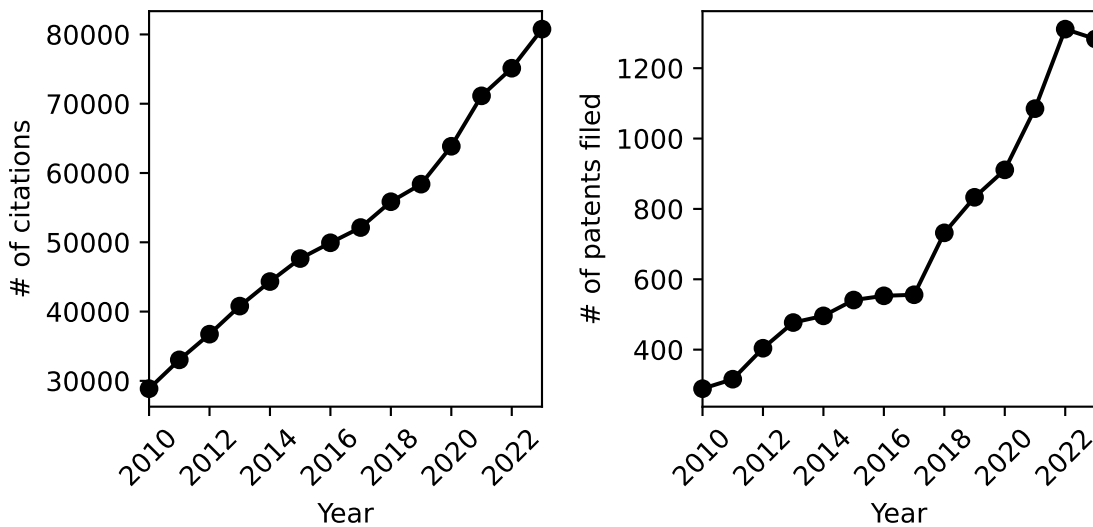


Figure 1: Number of citations^{1,2} (left panel) and patents (right panel) filed using significant CMS codes.

from the `atomistic.software` website,^{1,2} are based on the Google Scholar tracking engine. The number of patents is also drawn from Google Patents. Similar trends are reported by

other research groups,^{3,4} adopting bibliometric analysis of subjects such as density functional theory (DFT), which is the theory underlying a significant part of the CMS simulations.

The growth of annual citations of CMS codes is exponential with an approximate doubling time of about 9.5 years. The number of patents citing CMS codes is much smaller ($\approx 1,300$ vs. 80,000 in 2013) but the growth is faster (doubling almost every 6 years). This is faster than the overall scientific publishing counts, which is growing at about 4-5% per year with a doubling time of about 15 years.⁵ Clearly, both the development and application of CMS codes is of significant and increasing importance.

The growth of CMS as a field is mainly driven by two major factors. The technological factor, pertaining to hardware and the incredible increase in the available computing power, demonstrates a recent doubling time of about 20 months.⁶ The computational factor, on the other hand, focuses on the continual development of the underlying theory and practical implementations in software. Optimal control in both factors allows researchers to perform more accurate calculations on a larger scale that cover a wider range of practical use cases.

How are CMS codes used in practice? Individual codes are often adopted to simulate a physical system, e.g. a molecule or collection of molecules, a fluid, a crystalline or an amorphous solid, in order to predict its structure and properties, such as energy, band gap, or spectra. These simulations have many use cases. They can be used to explore systems of interest, to gain a better understanding, to help interpret and guide experiments, or to predict various properties, which often inform downstream or secondary student models. In some cases, a single code and type of simulation is sufficient to obtain a preset threshold of accuracy for simple and small systems. However, often numerous simulations, performed using different codes, are required to study and analyze the properties of larger and more complex systems. For example, optimizing the components of a battery might require quantum chemical simulations to determine reduction potentials, molecular dynamics simulations to predict diffusion constants and ionic conductivity of the electrolyte, and vibrational thermodynamics from phonon calculations to predict the entropy coefficient of anode and cathode

materials for the reversible volumetric heat source term in battery thermal models.

It usually takes tens or hundreds of simulations to understand the system, discover the hidden patterns within a measured set of properties and optimize these properties under certain conditions for practical purposes. Data management is also a significant challenge for simulations, as it requires careful tracking and documentation of the tools, methods, and parameters used. Furthermore, data management practices directly affect the reproducibility of the generated results and the extensibility of the performed simulations to new molecules or materials. At the end of the scholarly research process, the downstream tasks such as writing reports, manuscripts, or patents summarizing the results of the experiments will also be affected by the data management practices.

Some projects are handled by a single researcher, but others may require a team of researchers with computational and experimental backgrounds in different parts of the problem. Some researchers might handle the simulations, while others use the results to interpret and assist experiments or as input to other models that operate at different length and time scales. This collaboration increases the need for careful organization and tracking of the artifacts of the simulations.

However, CMS codes are not easy to use: the underlying theory is complex and the resulting equations are difficult to solve exactly except for the simplest "toy" systems, leading to many different approximations to the exact equations. Quantum chemistry codes have a range of methods from Hartree-Fock and DFT, which have larger approximations but are less computationally expensive, to coupled-cluster methods and full-CI, which are computationally very expensive but are closer to the exact solution. In DFT, the exact functional is not known, so there are numerous approximate functionals available. Most quantum codes make another approximation by expanding the wavefunction in terms of basis functions, which are typically Gaussian functions for molecules or plane waves for periodic systems. There are hundreds of different Gaussian basis sets in use.⁷ molecular dynamics (MDs) codes are also complicated with many choices of forcefields or atomic potentials, many different algo-

rithms to simulate different ensembles, and a wide variety of analyses. This complexity is unavoidable in any code trying to unravel chemistry and physics at the atomic level.⁸

This complexity is obvious in the input files that the user must prepare to run a simulation. There are a daunting number of input parameters to choose from. Some combinations of parameters may be allowed and others not, and if one parameter is set to a certain value, others may need to be adjusted to be compatible. Major quantum chemistry codes such as GAUSSIAN^{9,10} and GAMESS¹¹ have hundreds up to a few thousand keywords to choose from. the Vienna Ab initio Simulation Package (VASP),¹²⁻¹⁵ an electronic structure code widely used in the materials field, has about 46 main keywords, many of which have suboptions, yielding hundreds of combinations. This complexity is not restricted to quantum calculations: a Large-scale Atomic/Molecular Massively Parallel Simulator (LAMMPS),^{16,17} an MD code that is also widely used in the solid-state field, has over 1,000 commands, many of which have suboptions. It takes time and effort (and considerable trial and error) to learn how to use one of these simulation codes correctly and effectively. Unfortunately, while experience with one code lowers the barrier to learning a similar code, it only reduces it a moderate amount because the input and output of different codes are quite different. Experience with one class of codes is very little help in learning to use a different type of code. Many expert users of quantum chemistry codes are not comfortable with MD codes, and *vice versa*. Similarly, users of solid-state codes such as VASP face a considerable barrier with quantum chemistry codes, and *vice versa*.

The same issues make it difficult to compare codes or to reproduce or replicate the work of other researchers. It is challenging to include enough detail, even in the supplementary information, to be able to reproduce the results using the same code. It is considerably more difficult to replicate results with a different code, since that requires good working knowledge of the original code to understand the details of the simulation and expertise in the second code to set up a comparable simulation.¹⁸

These barriers impede all aspects of the CMS fields. The learning curve to become

proficient with CMS limits the use of the tools and makes it more difficult to use multiple codes to address larger and more complex problems. Leveraging previous work to accelerate current work is less likely when the previous results cannot be reproduced. Both the learning curve and the difficulty with reproducibility make it more difficult for researchers to use the best tool for the problem. It is hard to compare codes, and switching to a new code is costly, so there is a tendency to continue using known codes even if they not as effective for a particular problem or if they are computationally more expensive. These barriers also slow the development of new and better codes for similar reasons.

Despite the issues, the use of CMS codes is increasing with time. Any steps that reduce the learning curve, let users access more of the wide range of powerful tools available, install the software more easily, and make results more reproducible and easier to compare between codes will benefit users and further accelerate the use of these codes on significant scientific and engineering problems. This will also benefit the community developing the codes, challenging them to strive for more capable and more efficient software.

Existing Solutions

There are many efforts and codes that address the issues outlined above, indeed more than can be covered in detail here. This section will give examples of the most commonly used codes and how they fit the practical outline of how computational campaigns are structured. Starting at the lowest level, that is, the simulation codes themselves, progress is being made in standardizing parts of the input for quantum chemistry codes. For example, `libxc`¹⁹ is a library of DFT functionals currently used by more than 40 CMS software packages. `libxc` provides standard names for more than 600 functionals and ensures that the implementation is identical. Similarly, the Basis Set Exchange (BSE)⁷ is an open library of Gaussian basis sets for quantum chemistry. The BSE defines a standard naming and implementation for more than 700 basis sets. `libxc` and the BSE are steps in the right direction but account for only two of the input parameters to quantum codes, although both parameters are key and

have many possible values. The KIM project²⁰ and the associated OpenKIM website²¹ are examples of efforts to standardize the atomistic potentials used by MD codes for materials science.

There are a number of codes for constructing and visualizing molecular and crystal structures. Some examples are Jmol/JSmol,²² PyMol,²³ RASMOL,²⁴ VMD,²⁵ OVITO,²⁶ VESTA,²⁷ and CrystalMaker.²⁸ There is considerable variety in these codes. Some focus on molecular structures; others focus on crystal structures; and some on visualizing large-scale MD runs. Most are open-source, but CrystalMaker and PyMol are commercial products. Most, but not all, of PyMol is released under an open-source license. Some have tools for building structures, and a few can create the input files to run simulations with select codes. Building and visualizing structures is a key part of most simulations.

Another group of tools assist with setting up the input for calculations for a specific code or group of codes. Most can visualize systems, have building and editing tools for the structures, and provide a graphical user interface (GUI) for setting the parameters for the calculation. Avogadro^{29,30} is powerful and general, handling molecular and periodic systems, with good capabilities for building structures, analyzing results, and interfacing to a number of codes via a plug-in architecture. Other graphical interfaces support a single code, such as GaussView³¹ for GAUSSIAN, or for a set of similar codes, for example, Gabedit.^{32,33} These codes are designed to handle one calculation at a time. A structure is read from a file or created using a builder, and then the calculation is set up and run. Many of the codes can read the output of the calculation and display the results graphically. For example, many of these tools for quantum codes can display orbitals and electron densities. The combination of graphical builders with GUIs to run calculations is an excellent approach for exploration and getting started in a new project. An advantage of setting up a calculation for a specific structure is that the interface can be tailored to the problem at hand, offering only relevant choices. However, using this type of code is tedious and error-prone for running calculations on more than a few structures, since the calculation must be manually set up and run for each

new system. These codes handle more of the tasks needed for a computational campaign, but only cover some of the needed tasks.

A final class of codes, or environments composed of several codes, handle running many identical or similar calculations. Most of these codes provide a library of functions for common modeling tasks such as reading or building structures and running simulation codes. The user writes e.g. a Python script that sets the parameters and calls the library functions to run the calculations. This approach avoids the labor of repetitively setting up calculations for each structure and reduces the errors in manual approaches. Examples of these codes are AFLOW,³⁴ AiiDA,^{35,36} automated quantum mechanical environments for researchers and educators (AQME),³⁷ Atomic Simulation Environment (ASE),³⁸ atomate,³⁹ BigChem,⁴⁰ Digichem,⁴¹ MOSDEF,⁴² pyiron,⁴³ QCARCHIVE,⁴⁴ QMFlows,⁴⁵ and wfl.⁴⁶ Some of these codes, such as AiiDA and QCARCHIVE store results in a database, organizing the results for easy access. Databases are a very powerful tool for organizing extensive datasets, but are a challenge for most scientists to install and maintain, so the database-centric environments are most useful for expert groups preparing large datasets for machine learning, forcefield development, or public databases.^{47,48} The environments that do not depend on a database, such as a ASE, are easier for scientists to install and use, but they leave the organization of the simulations and results to the user.

Simulation Environment for Atomistic and Molecular Modeling (SEAMM)

The goal of the Simulation Environment for Atomistic and Molecular Modeling (SEAMM)^{49,50} as an open source software is to facilitate and enhance computational campaigns by automating many aspects such as the individual simulations, organizing the results so that they can be viewed and analyzed by any team member, ensuring reproducibility, and tracking citations for the codes and data used. In particular, SEAMM has the following goals:

1. Improve the productivity of users of atomistic simulation codes.
2. Make codes easier to use and less prone to errors.
3. Expand the range of codes that researchers can use by lowering the entry barrier.
4. Organize all inputs and outputs of simulations both to aid users and collaborators in viewing and analyzing the results and to ensure reproducibility.
5. Track all workflows to ensure that results across a computational campaign are consistent and comparable and can be extended as needed.
6. Track all codes and auxiliary data such as basis sets and forcefields, used in the workflow, to help correctly cite and credit their authors.

Example 1

Before covering the components and architecture of SEAMM, a simple example will be illustrative from the user's perspective. This example will show how to use MD in SEAMM to predict the density of ethanol at room temperature and pressure. At the heart of SEAMM are flowcharts, which encapsulate a reproducible workflow as a number of steps. Figure 2 shows a flowchart for creating a box of ethanol molecules as the model of the liquid and then using MD to predict its density.

This simple flowchart has three steps: selecting the forcefield to use, building the liquid ethanol model using PACKMOL to create a cubic cell containing a few hundred molecules of ethanol, and then running a constant pressure MD simulation using LAMMPS.

The user interacts with two parts of SEAMM:

- A graphical editor which can retrieve flowcharts from libraries, create them from scratch, edit them, and submit them as a job to be executed.

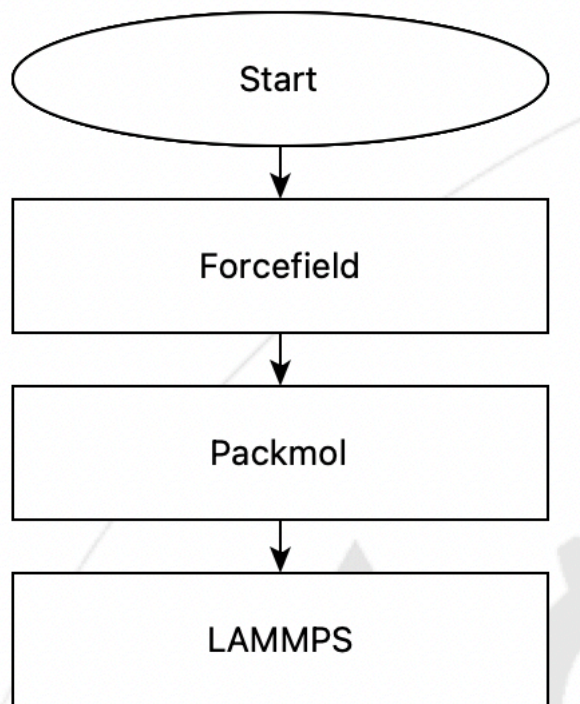


Figure 2: A sample flowchart for predicting the density of liquid ethanol via NPT MD simulation

- One or more web-based dashboards that handle the execution of the flowcharts and the data storage, tracking the jobs and monitoring of the results.

The flowchart in Figure 2 is created using the SEAMM GUI. The GUI provides a menu of steps. When the user adds a step, it is automatically added to the end of the flowchart queue, though it can be moved elsewhere if needed. The parameters for each step are edited using a dialog window provided by the step. The dialog window for configuring the PACKMOL step parameters is shown in Figure 3. In this example, the model is a cubic periodic cell containing a reasonable number of molecules of ethanol. The default values provided in the dialog window are very important for usability. By default, the PACKMOL step builds a spherical droplet with the size calculated from the initial guess of the density specified in the dialog and the number of molecules that contain about 2000 atoms. For this simulation, the first parameter in the dialog window should be changed for a cubic periodic cell, but the default number of molecules is already set to a reasonable value for the selected cell

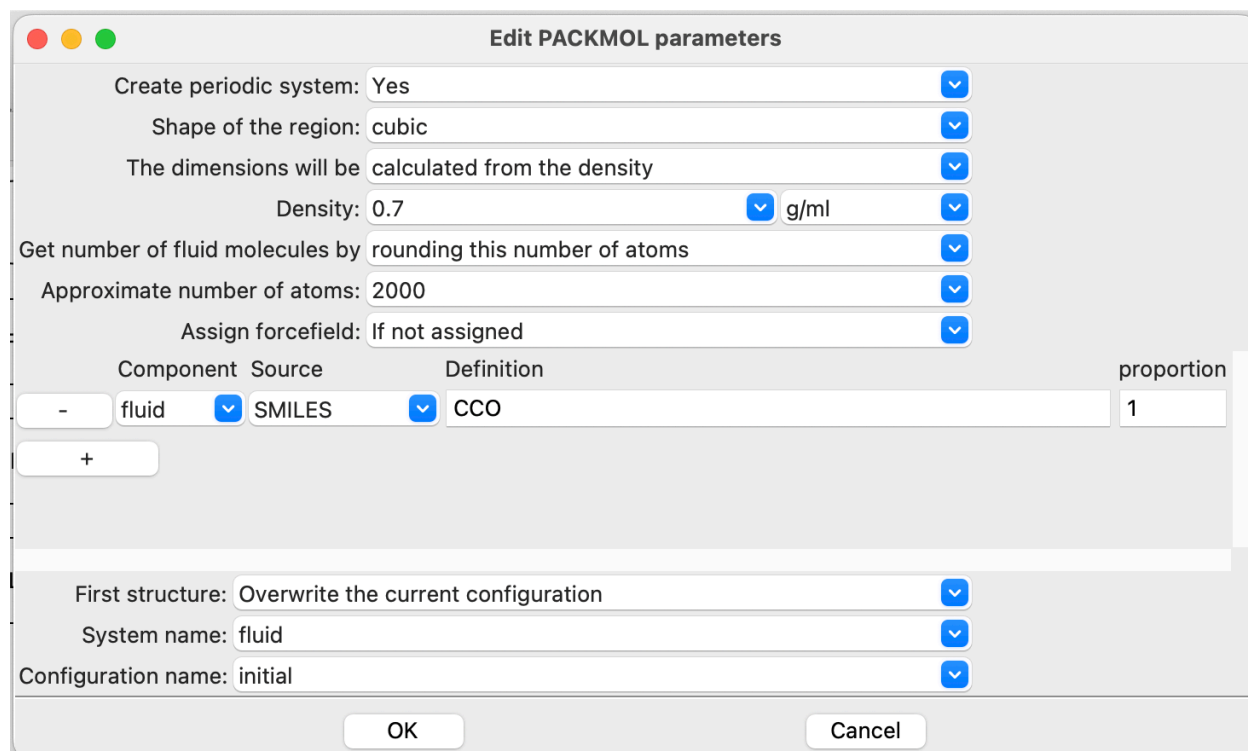


Figure 3: The PACKMOL parameter configuration dialog window in SEAMM

type. It is well-known that many properties from fluid simulations are sensitive to the cell size, converging as the size of the cell tends to infinity. The PACKMOL step uses this knowledge to guide and help users adopt good practices in their simulations. If the task was to compare the density of a number of compounds, say linear alcohols from methanol to decanol, SEAMM uses the number of atoms to determine the number of molecules to create cells of similar sizes. On the other hand, if different simulations used the same number of molecules, larger molecules would be simulated in larger cells which introduce systematic errors in the resulting comparisons. The design of the dialog window and the default values in it guide users towards simulations that will provide reasonable results with minimum computational costs. Although the PACKMOL step in the SEAMM flowchart creates the input (Figure 4) for running PACKMOL for the user, its interpretation requires a detailed knowledge of PACKMOL. Furthermore, the specific types of molecular structure files for input and output (here, PDB files) should be provided to PACKMOL by the user. In this example, SEAMM reads the Simplified Molecular Input Line Entry System (SMILES)⁵¹

```
1 tolerance 2.0
2 output packmol.pdb
3 filetype pdb
4 connect yes
5 structure input_1.pdb
6   inside cube 1.0000 1.0000 1.0000 26.9492
7   number 222
8 end structure
```

Figure 4: A sample input for PACKMOL

of ethanol, CCO, generates the system model for subsequent steps. The PACKMOL step in SEAMM also prevents another issue. PACKMOL does not create periodic cells. The documentation for PACKMOL recommends creating a somewhat smaller cell of the desired shape and transforming the created structure into a periodic system of the correct size. Using a somewhat smaller structure avoids creating atoms that are too close to each other when the system is transformed into a periodic cell. For ethanol, the PACKMOL step in SEAMM specifies a cube of dimension 26.9492 Å, which is then transformed into a cubic periodic cell of dimension 28.9492 Å containing 222 ethanol molecules. The generated model system has the initial guess for the density of 0.7 g mL⁻¹ based on the user’s request.

Controlling the LAMMPS step is similarly straightforward, with a dialog window for setting up the NPT dynamics as shown in Figure 5. Similarly to the PACKMOL step, the LAMMPS step also conceals considerable complexity and guides the user to a reasonable simulation. The input for LAMMPS is not shown here because the simulation control section in it is 115 lines of text long and the data describing the molecular structure and the associated forcefield parameters add 9415 lines to it. All input and output files from the LAMMPS step are available in the Supporting Information.

Once the flowchart is ready, the user can submit it as a job to any accessible running SEAMM Dashboard. The Dashboard may be running on the local machine or a remote powerful high-performance computing cluster intended for performing large-scale simulations. The job can be monitored on the Dashboard as it runs and the results examined as

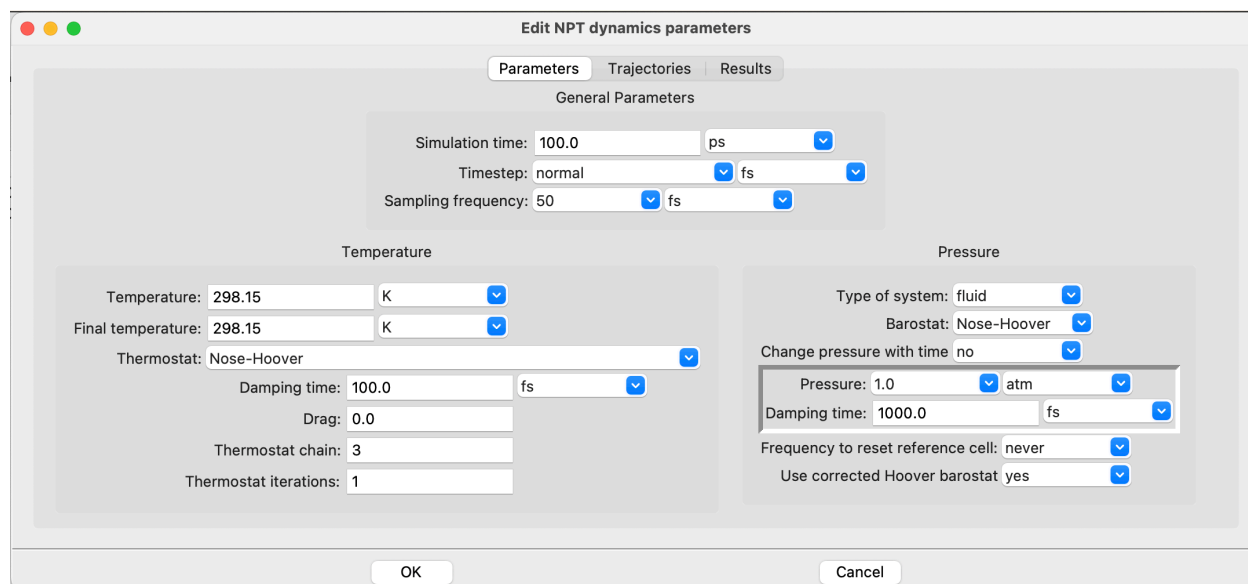


Figure 5: The parameters for LAMMPS.

they become available. For analyzing the job results, SEAMM offers two useful view modes: a textual summary output, shown in Figure 6, and the diagrams of state variables and calculated properties, such as line plots of the density and autocorrelation function, shown in Figure 7.

The summary output view is available for any step in a flowchart. It starts with a brief description of the main operation performed within the step alongside the control parameters that define the simulation. Next, a short summary of key results, are presented. In the example above, a table of the properties, derived from the NPT simulation along with the statistical error bars, an estimate of when the property converged to a steady state, the time constant of the autocorrelation function (ACF), and statistical inefficiency of the sampling, are provided in the results section of the summary output. The calculated density value of $0.791 \pm 0.001 \text{ kg L}^{-1}$ at 298 K and 1 atm is within about 1% of the experimental value of 0.79,⁵² using a high-quality forcefield such as Optimized Potentials for Liquid Simulations — All Atom (OPLS-AA).⁵³

In addition to the summary outputs, the Dashboard often offers other files that can provide more graphical details on property analysis or structure visualization. In this example,

```

Step 3: LAMMPS 2025.4.9
2 LAMMPS using MPI with 4 processes.
3
4 Step 3.2: Velocities
5 Set the velocities to give a temperature 298.15 K by using a random
6 distribution. LAMMPS will remove translational but not rotational momentum
7 The random number generator will be initialized with the seed '1692940359'.
8
9 Step 3.3: NPT dynamics
10 100.0 ps of canonical (NPT) dynamics at 298.15 K using a timestep of 1.0 fs
11 using the oplsaa+ forcefield. The temperature will be controlled using a
12 Nose-Hoover thermostat. The thermostat will use a chain of 3 thermostats
13 with 1 subcycles and a drag factor of 0.0. The pressure will be controlled
14 using a Nose-Hoover barostat.
15
16
17 The run will be 100,000 steps of dynamics sampled every 50 steps.
18
19 Analysis of npt_state.trj
20
21 Property Value StdErr Units convergence tau inefficiency
22 -----
23 T 298.113 ± 0.215 K 1.00 ps 53.1 fs 3.1
24 P 13.032 ± 29.292 atm 0.00 fs 25.0 fs 1.0
25 V* 21464.385 ± 26.524 Å3 31.00 ps 415.3 fs 17.6
26 density* 0.791 ± 0.001 g/mL 28.00 ps 430.8 fs 18.2
27 a* 27.793 ± 0.013 Å 28.00 ps 431.5 fs 18.3
28 b* 27.793 ± 0.013 Å 28.00 ps 431.5 fs 18.3
29 c* 27.793 ± 0.013 Å 28.00 ps 431.5 fs 18.3
30 Etot 2017.643 ± 3.312 kcal/mol 23.00 ps 124.3 fs 6.0
31 Eke 1774.646 ± 1.276 kcal/mol 1.00 ps 53.1 fs 3.1
32 Epe* 243.060 ± 4.770 kcal/mol 37.00 ps 369.4 fs 15.8
33 Epair* -1172.519 ± 3.049 kcal/mol 81.00 ps 201.4 fs 9.1
34
35 * this property has less than 100 independent samples, so may not be accurate.
36
37 The structure was added as a new configuration of the current system
38 named '' / 'simulated with oplsaa+'.

```

Figure 6: The summary output from the LAMMPS step.

SEAMM creates a diagram for each calculated property. The left panel in Figure 7 shows the line plot of the density simulation versus the time steps. Note the solid black line in the density diagram, indicating the average density calculated over the steady state simulation interval between 28-100 ps. The average density value is also presented in the textual output summary shown in Figure 6 above. The right panel in Figure 7 shows the ACF of the density in red with the error bounds shaded. The dark gray line is the best exponential fit to the ACF corresponding to the simulation time period reported in the summary output. These diagrams provide a rapid qualitative check on the calculation results, presented in the summary output. Furthermore, the ACF and the accompanying statistical inefficiency metric, which is a measure of oversampling of the trajectory, provide key information to improve the simulation, if necessary.

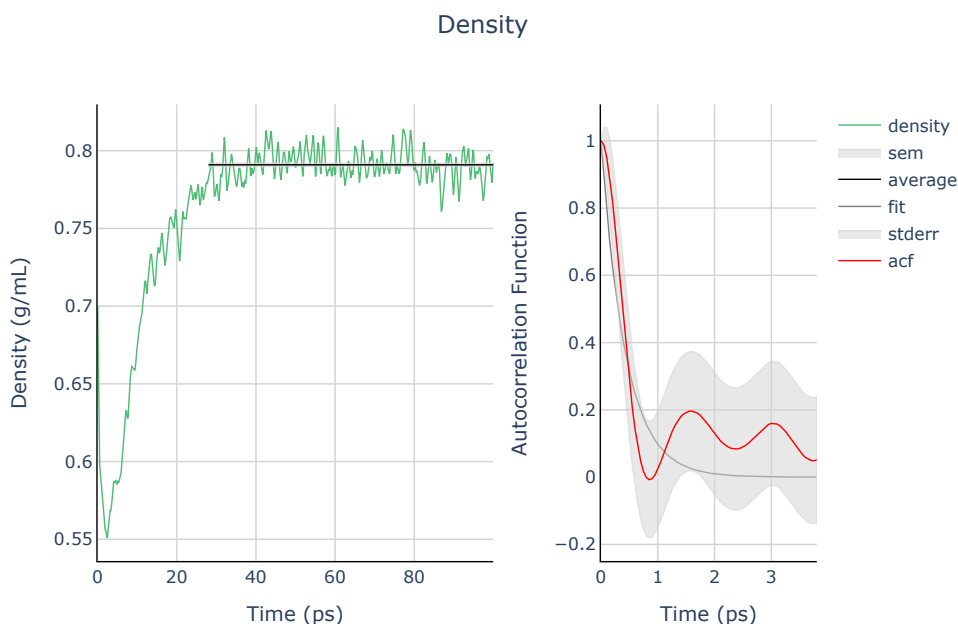


Figure 7: The line plots of the density (left) and the autocorrelation function (right) versus time, generated by the LAMMPS step in SEAMM. Note the horizontal line which SEAMM automatically creates on the density plot to represent the mean density value on the plateau.

Note that by changing the SMILES string in the PACKMOL step, the flowchart can be applied to other liquids, and mixtures can be simulated by adding additional molecules to

the component table. SEAMM supports runtime variables in flowcharts, which are set on-the-fly when submitting the job and can be used anywhere in the flowchart instead of pre-set constants. Generalizing flowcharts using runtime variables enables SEAMM to predict the density of any liquid consisting of any molecule that the forcefield can handle.

SEAMM and the plug-ins provide the summaries of the steps in the workflow, as well as appropriate citations for the codes and parameter sets used, both as text and as `BIBTEX`. This feature reduces the required effort for documenting the simulation details and providing a comprehensive description of the workflow. In the example shown above, the output and citations can easily be converted into the following sample description for scholarly publications: *The SEAMM environment⁵⁴⁻⁵⁶ was used to predict the density of ethanol at 298.15 K and 1 atm via an MD simulation with an isothermal-isobaric (NPT) ensemble using a Nose-Hoover thermostat/barostat,⁵⁷ running for 100 ps with a 1 fs time step using time-reversible, measure-preserving Verlet and rRESPA integrators⁵⁸ with the LAMMPS code.^{16,59} The potential energy of the system was calculated using the OPLS-AA forcefield⁵³ with custom parameters for ethanol obtained from the LigParGen website.⁶⁰⁻⁶² Non-bonded interactions were cut off at 10 Å with long-range Coulomb terms handled using a particle-particle particle-mesh solver⁶³ and a tail correction⁶⁴ for long-range Lennard-Jones terms. The model of liquid ethanol was a cubic periodic cell containing 222 molecules of ethanol. The initial structure was created using PACKMOL^{65,66} to create a cubic cell with a density of 0.7 g/cm³ using an ethanol structure created from SMILES using OpenBabel.^{67,68} The analysis of the trajectory was carried out by the LAMMPS step⁵⁵ in SEAMM, using the pymbar library⁶⁹⁻⁷² to determine when the system had reached a steady state and to perform the statistical analysis of that portion of the trajectory.*

SEAMM Components

Figure 8 provides a high-level view of various parts of the SEAMM environment. The next few subsections will provide more details on each components and how individual parts work together to provide a comprehensive software ecosystem for performing CMS simulations.

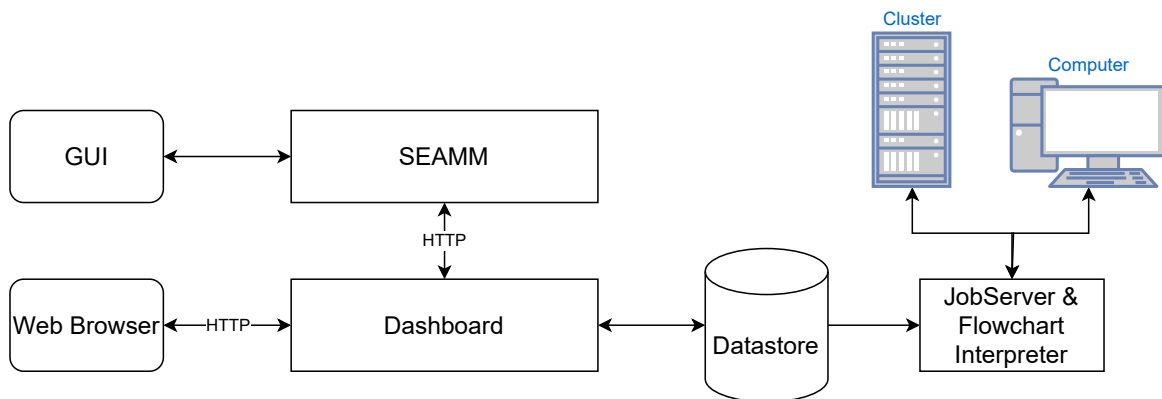


Figure 8: Components of the SEAMM environment.

SEAMM Core

Figure 9 shows SEAMM, which is the central part of the SEAMM environment in Figure 8, in more detail. There are five parts: a database for storing computational results during a job, a GUI and utility libraries that contain useful functionality for developers, an Application Programming Interface (API) that defines the interface between SEAMM and the plug-ins, which provide all the functionality that users see, e.g. the flowchart and dialogs in Example 1.

Plug-ins

SEAMM, at its core, is a framework that provides its own data model and numerous utility functions without offering any end-user functionality. In order to enhance modularity, SEAMM directs external end-user functionalities into separate code units, called plug-ins, as shown in Figure 9. Each plug-in corresponds to a step in a flowchart. Plug-ins provide

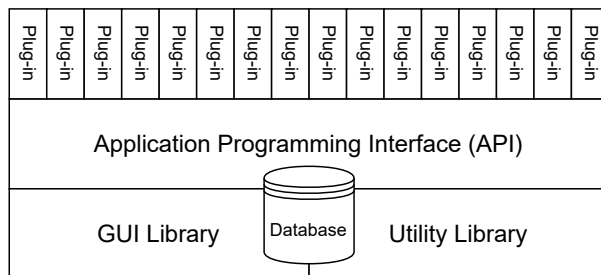


Figure 9: High-level software stack view of SEAMM core component

interfaces to external CMS simulation tools, builders for creating systems, analysis modules, control steps in flowcharts such as loops and sub-flowcharts, and other functionality that users need to run their simulations. Plug-ins are developed based on SEAMM API but are independent software modules and distributed separately from SEAMM. SEAMM installer finds the plug-ins, published on the Python Package Index (PyPI),⁷³ and installs or updates them upon user request.

In Example 1, the three steps in the flowchart in Figure 2 correspond to individual plug-ins that provide interfaces for the PACKMOL, LAMMPS and the forcefield steps. When the flowchart is executed, the forcefield step plug-in reads the forcefield from a disk file and stores it in internal data structures for easy access. A substantial part of the utility library is devoted to handling forcefields, including automatic “atom typing” and preparing the lists of forcefield parameters for codes such as LAMMPS. As such, the forcefield plug-in can automate most aspects of forcefield development for both users and developers, as detailed in Example 1, where the user only had to choose which forcefield to they want to use and everything else related to the forcefield was hidden.

Data Model and Internal Database

SEAMM supports simulations of molecules, fluids, and amorphous and crystalline solids plus interfaces between different phases. Although these structures are closely related, different disciplines use different terminologies which can be confusing. Before proceeding with dis-

cussing data storage, we will cover the adopted terminology in SEAMM. The term “*system*” denotes a collection of atoms, molecules, and/or crystals that are simulated, analogous to experiments on thermodynamic systems.⁷⁴ In SEAMM, the *system* itself is an abstraction that consists of one or more *configurations*, which themselves are composed of atoms along with their coordinates, optional bonds between atoms, the periodic cell for periodic *systems*, the point- or space-group symmetries, and the charge and spin/magnetic states of the *system*. Many codes call what SEAMM refers to as a *configuration* a “molecule” or “structure”, or in some cases they are “conformers” or “frames” in a MD trajectory. The *configurations* in SEAMM are more general than the structures or the frames in trajectories in most codes. Different *configurations* of a *system* can have different atoms and different bonds. With this flexibility, SEAMM can support reactive dynamics and other simulations of chemical reactions in a natural way. SEAMM can also support grand canonical ensembles, where the number of atoms or molecules can change such as when simulating vapor deposition by creating a stream of new molecules to impinge on a target surface.

Most quantum codes take the charge and spin as input parameters for the simulation. In SEAMM, charge and spin multiplicity are properties of the *configurations*. This feature extends the usability and generality of flowcharts to handle neutral molecules, anions, cations, and different spin states within the same framework. Chemists think of singlet and triplet oxygen as two different chemical entities, as does SEAMM.

SEAMM uses the concept of a *subset*, which is an arbitrary collection of atoms in a *configuration*. Atoms can be in more than one *subset*, which allows *subsets* to be defined for commonly used concepts such as residues and chains in proteins or adsorbents and adsorbates. *Templates* are closely related to *subsets* but contain a *configuration* that has atoms, bonds, and coordinates, as well as other useful attributes such as names, partial charges, and forcefield atom types. A *template* is a prototype that can be used to find identical substructures in a *system*, matching them atom-by-atom regardless of the order of the atoms. Once matched, attributes such as atom names, partial charges, and bond orders can be transferred

from the *template* to the substructure. For example, *templates* of the amino acids could be used to match the different residues in a protein and provide the structure with standard names, partial charges, and atom types.

The data for *systems*, *configurations*, *templates*, calculated properties and other results are stored in an internal relational database. Rather than accessing the database directly, the utility library provides a facade over the database, so to the rest of the SEAMM and to the plug-ins, the underlying data model is accessed through an object-oriented framework with *systems*, *configurations*, atoms, bonds, etc. This model is common in simulation codes, so developers will probably find this aspect of the SEAMM similar to other software packages they may already be familiar with.

There are several advantages to using a relational database. Relational Database Management Systems (RDBMSs) constitute a mature, well-understood, high-performance and scalable technology. SEAMM currently uses SQLite⁷⁵ for database management because it is small and lightweight, well-integrated with Python, and designed for use within programs. Since structured query language (SQL) is a standard language for RDBMSs, including SQLite, SEAMM could switch to a different SQL-based RDBMS if needed. A second advantage, particularly of SQLite, is that the database file is portable across platforms, storing data with full precision fidelity. As such, SEAMM and the database files are also portable across different hardware and operating systems. Furthermore, the most important advantage gained is the flexibility and extensibility that a database provides.

The schema used in the database defines the data that it stores as tables, columns, and relations between them. There are two main parts to the schema used by SEAMM: a conventional schema for *system* and *configurations*, and a star schema⁷⁶ for property data and simulation results.

Figure 10 shows the schema for *system* and *configurations*. The *configuration* is the heart of the description, connected to the atoms and bonds through the junction tables `atomset_atom` and `bondset_bond`. This allows *configurations* to contain different atoms or

bonds, while avoid duplicating the shared atoms and bonds for storage size reduction. The data storage size is important for large MD simulations with extensive trajectories. Storing the atomic coordinates separately from other atomic features also helps limit the amount of data stored during MD simulations, since in many simulations, the topology of the structure—atom types and bonds—do not change, but the atomic positions change with every step. The remainder of the schema is the handling of the point or spacegroup symmetry and periodic cells with three tables at the top, and *subsets* and *templates* in the lower left portion of the diagram.

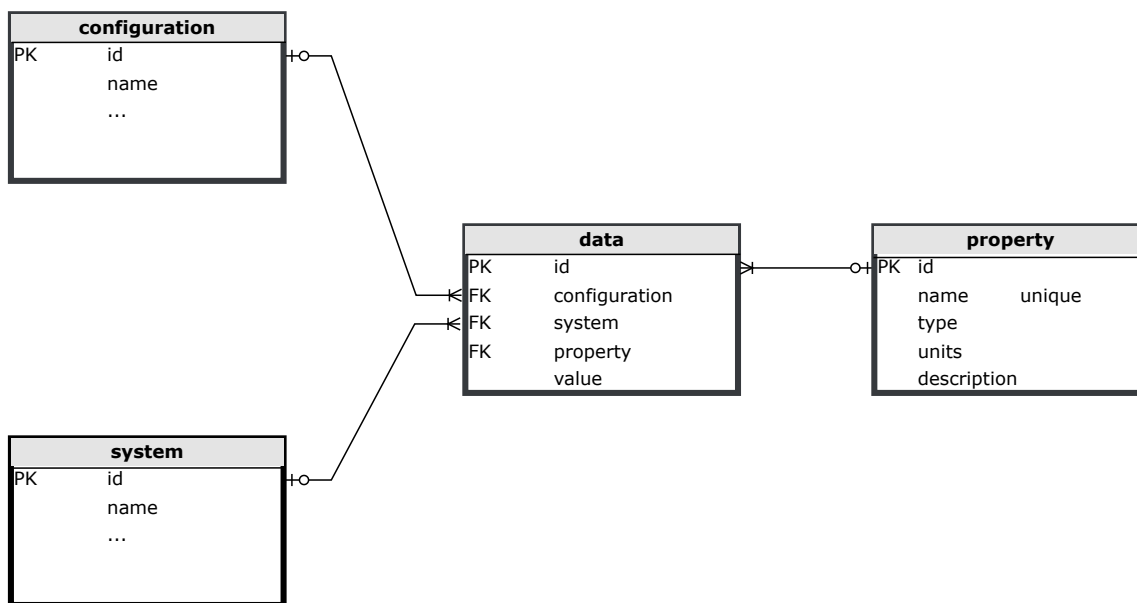


Figure 11: Star schema for system properties

The second part of the schema is the star schema for handling properties and calculated results, shown in Figure 11. The values of the properties and other results are stored in the `data` table. In a conventional schema, the table would have a column for each property, such as energy, dipole moment, band gap, etc. This is not practical because the number of different results from all possible simulations is large but each specific simulation generates only a small number of different results. This would require an extremely wide table that would only be sparsely populated. Adding a new type of result would require changing the

schema, versions of database, *etc.* which is unsustainable.

The star schema circumvents this problem by using metadata to describe the data in the `data` table and storing the metadata in the `property` table. As such, the `data` table remains dense. Adding a new property or type is also possible by inserting a new row of metadata to the `property` table, which can be done while SEAMM is running, without the need for any change to the code requiring a new release. The disadvantage of the star schema is that finding data requires several layers of indirection or “join” operations in SQL vocabulary. Fortunately, RDBMSs are highly optimized for performing join operations because star schemas are widely used in commerce to store data, such as credit card transactions or airline reservations, which require high-performance and truly massive databases but similarly sparse data.

Similar to the database that stores the structures, SEAMM provides an object-oriented facade over the star schema. The facade provides methods to define new properties, to add property data to *systems* and *configurations*, and to search for and retrieve the data. SEAMM defines standard properties such as electronic energy, formation enthalpy, dipole moment, volume or band gap, providing a *de facto* standard. The plug-ins can dynamically add any other properties that they need, such as thermal expansion coefficient, heat capacity or viscosity, though if another plug-in needs the data, the plug-ins must agree on a consistent and common naming convention.

It is impossible to overstate the importance of flexibility and extensibility of the data management systems for handling a wide range of tools and applications in the CMS fields. It is also key in ensuring SEAMM’s ability to evolve, support new codes and enable new science for many decades to come.

Utility Library

The utility library contains a number of useful tools that can be assembled by plug-ins to meet specific needs such as:

1. A comprehensive package for handling units, based on the open-source Python package Pint⁷⁷ and customized to handle unit conversions that are common in chemistry and materials science;
2. interfaces to Open Babel,⁷⁸ RDKit,⁷⁹ ASE,³⁸ and geomeTRIC⁸⁰ to facilitate their use within the SEAMM environment;
3. functions to traverse the molecular graphs defined by the bonds between atoms to find individual molecules, neighbors of atoms, angles, dihedrals, and other topological features of molecules;
4. handling of the forcefield files; and
5. a flexible printing system modeled after the Python logging system.

GUI Library

The GUI in SEAMM is implemented using a model-view-controller (MVC) design pattern, which allows multiple graphical implementations to be used interchangeably. The initial implementation is based on tkinter,⁸¹ which is Python's native GUI package. The GUI library in SEAMM provides a number of widgets that are tailored to the needs of CMS, such as periodic tables and entry fields that have built-in unit handling. These features make the development of the GUIs for SEAMM plug-ins easier and help standardize the resulting user interface and experience. There is also support for creating diagrams similar to those shown in Figure 7.

The SEAMM Application Programming Interface for Creating Plug-ins

Plug-ins consist of at least four components: a computational class that defines the core computational functionality of the plug-in; a graphical class that defines the graphical user

interface (GUI); a class that contains the parameters which are set by the GUI and consumed by the computational class; and a small factory class that SEAMM uses to instantiate objects of the computational and graphical classes. The first three classes are subclassed from base classes provided by SEAMM core. The factory class is minimal, consisting of two methods, each of which has a single line of code that creates and returns an instance of the compute or graphical class for the plug-in. The three base classes plus the factory class define and enforce much of the API for SEAMM. Python does not directly support virtual classes; however, base classes raise exceptions in methods that must be overridden in the subclass. These base classes also contain a number of methods that implement a significant portion of the functionality of a plug-in. In most cases, these methods are sufficient out-of-the-box, but can also be overridden for special cases.

SEAMM provides a Python Cookiecutter⁸² which is built upon the Cookiecutter for Computational Molecular Sciences.⁸³ The SEAMM Cookiecutter creates a directory and project for a new SEAMM plug-in. It is populated with the initial source files for the plug-in, a skeleton of the documentation, tests, and the files needed to create a complete project in GitHub including the GitHub Actions to check the code, run tests, and eventually release on PyPI. As such, the Cookiecutter greatly lowers the development barrier for creating plug-ins SEAMM and ensures their consistency with the SEAMM API. The initial skeleton, created by the SEAMM Cookiecutter can be installed and used immediately. However, it has no useful functionality on its own. Therefore, the developer's task is to add the required parameters, edit the dialog window if the automatic placement of the parameters is not sufficient, and create the code for executing the core function. For example, a plug-in that runs a simulation code needs to define the control parameters for it. The GUI code will automatically display the widgets for the parameters in a table, which is sufficient if there are only a few parameters. For more complex plug-ins the developer needs to change the code that positions the widgets and impose any dependencies between parameters if the value of one parameter affects the others. The developer must also create the code to take

the parameters and create the input for the simulation code, and also reformat the atomistic structure for the code. Finally, the code to run the simulation code, and read and analyze the output also needs to be written.

The developer must supply any codes, libraries, or data that are needed to run the simulation, and may need to write a simple installer for these items. SEAMM provides templates and utilities for such installers. At the very least, the plug-in must document how users can obtain and install any required code and data. If the dependencies are open-source or accessible in the public domain, the best practice is to ensure that the plug-in retrieves and installs everything that it needs. Simulation codes should be installed in separate Conda environments or Docker containers to minimize conflicts between different codes and their dependencies.

Dashboard and Datastore

Example 1 briefly showed the Dashboard from a user's point of view. The Dashboard is a custom web server for monitoring and managing jobs. The jobs are stored in the datastore, which is a combination of a RDBMS and files on disk. The database stores information about the jobs as well as pointers to the disk files, allowing for rapid access. The inputs and outputs of the simulations are stored as files and indexed in the database. This allows users to directly access the files or use shell scripts and similar tools to access them if they wish. It also allows users to backup the files using tools that they are comfortable with, rather than trying to backup what would be a very large database if the simulation results were stored therein. The information in the database for each job is also saved in a disk file alongside other job files. The Dashboard can recreate the database from these files if it is corrupted.

The Dashboard provides a Representational State Transfer (REST) API to the datastore, allowing programmatic access to the data. The SEAMM GUI uses this API when submitting jobs to the Dashboard. Since this feature uses hypertext transfer protocol (HTTP) for data transport, SEAMM can access the Dashboard from anywhere via a browser. Users can also

access the Dashboard and jobs on any machine that they can access directly or through *e.g.* secure shell (SSH) tunneling.

JobServer

The JobServer is a daemon or long-running service is responsible for running jobs, submitted to the Dashboard, and placing them in the datastore queue. The JobServer accesses the datastore directly, periodically checking the queue for monitoring jobs that are waiting to run. The current version of the JobServer executes a job's flowchart directly on the machine or in a Docker image if SEAMM is installed using Docker. Future versions will be able to work with queuing systems which are typically used on large computer clusters.

Flowcharts

Flowcharts are text files in JavaScript Object Notation (JSON) format that define the steps in each workflow, their control parameters and the connections between them. Each step in a flowchart corresponds to a plug-in, represented by a graph node. The individual steps (nodes) are composed of three pieces of information defining the plug-in– the Python module of the plug-in, the class name, and the version of the plug-in– plus data that the plug-in defines and handles. This information allows a code, interpreting the flowchart, to instantiate each plug-in and have it read its internal information from the flowchart. The API for plug-ins specifies an `edit` method, which SEAMM uses to present the plug-in's dialog window to the user, and a `run` method, which handles the actions of the plug-in. SEAMM also provides an interpreter to execute the flowcharts. Each flowchart starts with the appropriate shebang line pointing to the interpreter. Thus, if the flowchart file is executable, it will run if called directly within a command-line interface.

This design provides a great deal of flexibility. Because the version of each plug-in is recorded in the flowchart, it is possible to use either the latest version of the plug-ins, or the version specified in the flowchart. Since plug-ins are responsible for handling their own

data in the flowchart, they are free to store their data in any convenient form, regardless of data management aspects in any other part of SEAMM. Because flowcharts are text files, they can be shared by email, saved to disk, or placed in libraries. SEAMM can publish flowcharts on Zenodo,⁸⁴ a free and open-source research repository developed by CERN and OpenAIRE, which assigns the flowcharts a digital object identifier (DOI) for future reference. Flowcharts can also be searched on Zenodo and be downloaded directly into SEAMM.

Example 2: Rearrangement of Methylisocyanide to Acetonitrile

One of the strengths of SEAMM is its ability to use a range of codes to tackle complex multi-scale problems in CMS. This section will focus on the rearrangement of methylisocyanide to acetonitrile, which is a prototype for unimolecular reactions and has been studied extensively, both experimentally and computationally.⁸⁵⁻⁸⁹ We will reproduce the results of one of the early computational studies⁸⁸ and then replicate the results using a wide range of computational methods in SEAMM. The focus will be on the energy of the transition state structure and the curvature of the potential energy surface at the saddle point.

We will start by reproducing the optimized transition state structure and its harmonic vibrational frequencies as provided in Ref. 88 and then move to locate the transition state structure from scratch. Given the structure, it is straightforward to calculate the vibrational frequencies and the normal modes using quantum chemistry software such as GAUSSIAN¹⁰ or PSI4.⁹⁰ The results are shown in Table 1.

The first column lists the reference frequencies obtained from Ref. 88, where the second derivatives needed for the harmonic vibrational analysis were calculated using finite differences of gradients. The second and third columns in Table 1 show the vibrational frequencies calculated using `gaussian` and PSI4, respectively, using analytic second derivatives. The analytic frequencies are identical to those of Ref. 88 within less than 1cm^{-1} while the ener-

Table 1: The vibrational frequencies (cm^{-1}) and energies (E_h) of the transition-state structure for the rearrangement of methylisocyanide to acetonitrile calculated at the HF/DZP level of theory. The reference values are obtained from Ref. 88

	Ref. 88	GAUSSIAN	PSI4	Finite Difference
Frequencies (cm^{-1})	458 <i>i</i>	458 <i>i</i>	458 <i>i</i>	459 <i>i</i>
	255	255	255	255
	677	677	677	677
	1063	1063	1063	1063
	1083	1083	1083	1083
	1457	1457	1457	1456
	1590	1590	1590	1589
	1599	1599	1599	1599
	2189	2189	2189	2189
	3272	3272	3272	3272
	3388	3388	3388	3388
	3411	3411	3411	3411
Energy (E_h)	-131.84756	-131.84744	-131.84738	-131.84744

gies are in perfect agreement within $0.0002 E_h$ (or $\approx 0.13 \text{ kcal mol}^{-1}$). The different codes make different approximations to reduce the computational cost. For example, PSI4 uses the resolution of identity (RI) and various cutoffs by default when evaluating the two-center integrals. GAUSSIAN, on the other hand, does not use RI. As noted in Ref. 88, the code used at the time could not handle the d functions in the basis set. As such, the d functions were approximated by off-center p orbitals which introduced an error of $\approx 0.0001 E_h$. Note that such errors or approximations tend to be systematic. Thus, relative energies are more meaningful and accurate in this context. In this section, we have made no effort to tune the input parameters in PSI4 and GAUSSIAN and benefited from reasonable default values in SEAMM to reduce the errors from the approximations made to gain performance. The the precision of the current results is also well within chemical accuracy and on-par with the precision of the original calculations performed more than 40 years ago. These results provide strong evidence for the reproducibility of the quantum chemical calculations between different codes with quite different implementations and running on very different computers which stood the test of time over decades.

Both GAUSSIAN and PSI4, as well as a number of other codes, with available interfaces in SEAMM, can calculate second derivatives analytically. However, many codes may not offer this feature. The `Thermochemistry` plug-in in SEAMM eliminates this issue by using finite differences or the first derivatives to calculate harmonic vibrational frequencies and properties. The last column in Table 1 shows the results of the finite difference approach mentioned above using GAUSSIAN to calculate the energy and first derivatives. Using the default step size of 0.01 Å in the `Thermochemistry` plug-in, the results are essentially identical to those calculated analytically, with a deviation of 1 cm⁻¹ in the frequencies. Another advantage of using the `Thermochemistry` plug-in is that it ensures that the vibrational analysis is handled identically when using different methods and codes. As an added benefit, the `Thermochemistry` plug-in makes it easy to switch between different simulation codes, since only a small subflowchart, responsible for calculating the energy and forces, needs to be changed.

Beyond reproducing the results for the given transition state structure, the `Reaction Path` plug-in for SEAMM finds approximate reaction paths and transition states using the nudged elastic band (NEB) method.⁹¹⁻⁹⁵ Once an approximate transition state is located, the `Structure` plug-in can optimize it, in the process ensuring that there is one and only one mode with an imaginary frequency. Similar to the `Thermochemistry` plug-in, both plug-ins only need the energy and gradients of the structure, allowing them to be used with a wide range of simulation methods in SEAMM.

Table 2 shows the relative enthalpies of the structures in the reaction path, as well as the imaginary frequency of the transition state, calculated with a range of codes and methods, ranging from *ab initio*/ Hartree Fock method with Gaussian orbitals and numerical ones, semiempirical Hartree Fock methods in MOPAC, and semiempirical DFT using DFTB+. The *ab initio* Hartree Fock methods give almost identical results. The observed small differences are mainly due to differences in the quality of the analytical and numerical basis sets in various codes. The results presented in Table 2 demonstrate that the semiempirical methods,

Table 2: Comparison of the enthalpies (kcal mol⁻¹ at 298K and 1 atm) of the structures of methylisocyanide, the transition state, and acetonitrile relative to methylisocyanide, plus the curvature of the imaginary mode at the transition state for a range of different models.

	HF/DZP ^a	HF/tight ^b	PM6-org ^c	PM7 ^d	DFTB/3ob ^e	xTB/GFN2 ^f
CH₃NC	0.0	0.0	0.0	0.0	0.0	0.0
TS	43.6	42.5	60.5	73.1	60.2	62.8
CH₃NC	-19.5	-20.0	-29.5	-20.7	-10.4	-23.5
Freq.^g	458.0 <i>i</i>	463.0 <i>i</i>	577.0 <i>i</i>	696.0 <i>i</i>	343.0 <i>i</i>	412.0 <i>i</i>

^aHartree Fock with GAUSSIAN using the “DZP” basis. ^bHartree Fock with FHI-AIMS^{96,97} using the “tight” basis.⁹⁸ ^cHartree Fock with MOPAC⁹⁹ using the “PM6-ORG” parameterization.¹⁰⁰ ^dHartree Fock with MOPAC using the “PM7” parameterization.¹⁰¹ ^eDFTB¹⁰² with DFTB+¹⁰³ using the “3ob” parameterization.¹⁰⁴ ^fxTB¹⁰⁵ with DFTB+ using the “GFN2” parameterization.¹⁰⁶ ^gFrequencies are in cm⁻¹.

whether based on Hartree Fock or DFT, overestimate the reaction energy barrier height and have a larger variance for both the enthalpy of reaction and the imaginary frequency.

Similar calculations with ReaxFF forcefields^{107–109} and machine learning potentials^{110,111} could not locate the transition state, nor could the transition state be successfully optimized starting from the known transition state structure using these forcefields or potentials. Although details of the parameterization are difficult to track in these methods, it appears that the training data for all of the methods examined include cyanides but not isocyanides. Each of the potentials tried predicts a nonlinear C-N-C bond angle in methylisocyanide instead of the known linear structure, indicating that the extrapolation of the potentials to the isocyanide functional group is not reasonable. So, while SEAMM is capable of locating the transition state and calculating its thermochemistry using such potentials, for this particular reaction none of the forcefields or machine learning potentials tried in this study could represent the potential energy surface in a physically reasonable way, because the reactant and transition state are too far from the training sets. More details about the calculations and results in this example are included in the Supporting Information, along with a description of the flowchart used.

Example 3: Advancing Understanding of Battery Materials

SEAMM is not only a productivity software for reproducible CMS workflows and a powerful engine for academic research, but it is also a valuable tool for industrial research. In this example, we highlight a real-world application of SEAMM in predicting the transport properties of lithium ion battery materials via MD simulations. This study has two main parts. First, we will discuss the simulation of transport properties such as ionic diffusivity, conductivity, and transference number in liquid electrolytes such as EC:EMC (3:7 w/w) and EC:DMC (1:1 w/w) with LiPF_6 at room temperature. Second, we will discuss the thermal expansion in battery electrodes such as LiCoO_2 at finite temperature and their thermal conductivity as a function of the state of lithiation (SOL) at room temperature.

The performance of lithium-ion batteries at low temperatures or under rapid charge-discharge conditions is governed by the intrinsic transport properties of their liquid electrolytes. Despite their importance, even for conventional electrolytes, the available transport measurement data at various concentrations and temperatures are scarce in the literature. An alternative to measurement techniques is to simulate the system in order to predict the desired transport properties under various operating conditions that are not otherwise easily accessible through experiments. Here, we demonstrate the application of classical MD via the LAMMPS code to model transport in EC:EMC (3:7 w/w) and EC:DMC (1:1 w/w) electrolytes with various concentrations of LiPF_6 salt at room temperature. The simulations were performed using SEAMM flowcharts to build the MD input files, call the LAMMPS calculator, and finally use custom Python scripts for post-processing of the trajectory data.

Table 3 shows the SMILES of different solvents and the salt used in our simulations which are ethylene carbonate (EC), ethyl methyl carbonate (EMC), dimethyl carbonate (DMC), and lithium hexafluorophosphate (LiPF_6) salt. The initial MD configuration is generated using the PACKMOL step, which reads the SMILES strings of the solvents and salt based on

Table 3: Solvent and salt SMILES strings, experimental density and MD simulation density at 25° C

Solvent/Salt	SMILES	Exp. Density (g cm ⁻³)	MD Density (g cm ⁻³)
EC	C1COC(=O)O1	1.32	1.33
EMC	CCOC(=O)OC	1.01	1.03
DMC	COC(=O)OC	1.07	1.08
LiPF₆	[Li ⁺].F[P ⁻](F)(F)(F)(F)F	–	–

the given electrolyte formulation and creates a cubic periodic cell to initiate the LAMMPS simulation. The OPLS-AA force field^{112,113} were used to describe the bonded and nonbonded parameters of each solvent. The parameters used for the Li⁺ cations and LiPF₆ anions were from Jensen *et al.*¹¹⁴ and Lopes *et al.*,¹¹⁵ respectively.

The individual density of each solvent was first validated through MD simulations, as shown in Table 3. These densities were used to make an initial guess for the density and hence dimensions of the initial configuration of the electrolyte formulations. The LAMMPS simulation involved a structural minimization followed by 2 ns NPT canonical dynamics using a Nose-Hoover thermostat and barostat at 25° C and 1 atm to equilibrate the system. The cell was then adjusted isotropically to the equilibrium density and the results of 5 production runs of 200 ps of NVT dynamics were averaged. Using SEAMM’s `Diffusivity` module, the position and velocity trajectories were analyzed and the diffusion constant was calculated using the Mean Square Displacement (MSD) approach. The slope of the linear regime in the MSD was obtained for each simulation of 200 ps duration and averaged over the total of 1 ns of the production runs to obtain the diffusion constant, defined as

$$D(T) = \frac{\langle \text{MSD}(T) \rangle}{6\Delta t} \quad (1)$$

The electrolyte salt diffusivity, $D_{\text{LiPF}_6}(T)$, was calculated from the individual diffusivities of Li⁺ cations and PF₆⁻ anions in the cell as¹¹⁶

$$D_{\text{LiPF}_6}(T) = \frac{2D_{\text{Li}^+}(T) D_{\text{PF}_6^-}(T)}{D_{\text{Li}^+}(T) + D_{\text{PF}_6^-}(T)}. \quad (2)$$

The electrolyte ionic conductivity, $\sigma(T)$, can also be calculated using the Nernst-Einstein equation,¹¹⁷

$$\sigma(T) = \frac{N_{\text{Li}}e^2}{Vk_B T}(D_{\text{Li}^+}(T) + D_{\text{PF}_6^-}(T)), \quad (3)$$

where, N_{Li} is the number of Li^+ ions and V is the volume of the simulation cell, e is the electronic charge, T is the temperature, D_{Li^+} is the Li^+ cation diffusion constant, and $D_{\text{PF}_6^-}$ is the PF_6^- anion diffusion constant. The cationic transference is expressed in terms of the ratios of the ionic diffusivities,¹¹⁸

$$t_+ = \frac{D_{\text{Li}^+}}{D_{\text{Li}^+} + D_{\text{PF}_6^-}} \quad (4)$$

Figure 12 shows the calculated transport properties from MD simulations of EC:EMC (3:7 w/w) and EC:DMC (1:1 w/w) electrolytes, at various molar concentrations (c) of LiPF_6 salt at 25° C. The equilibrium densities [Figure 12 (a)], obtained from the MD simulation, are in agreement with the experimental mass densities of EC:EMC (3:7 w/w)¹¹⁹ and EC:DMC (1:1 w/w)¹²⁰ electrolytes, especially at salt concentration > 0.5 M. At any salt concentration, the EC:DMC (1:1 w/w) mixture resulted in a higher density values than those of EC:EMC (3:7 w/w). Landesfeind and Gasteiger¹²¹ performed an extensive experimental study on the temperature and concentration dependence of the ionic transport properties of these electrolytes. We compare the simulated ionic diffusivity, conductivity and transference number with their result as shown in Figure 12(b-d). We found that the predicted ionic transport properties from the simulation underestimated the experimental results, which could be attributed to the default ionic charges of the OPLS-AA force-fields. It has been reported in earlier literature that the transport properties in high-concentration electrolytes can be significantly underestimated if the ionic charge correction is neglected^{122,123} in the MD simulations conducted with OPLS-AA force-fields. Even using the recently improved OPLS4 force-field parameters,¹²⁴ the predicted values of transport and thermodynamic properties of various ions and solvated molecules of common ionic liquids for a wide range of tempera-

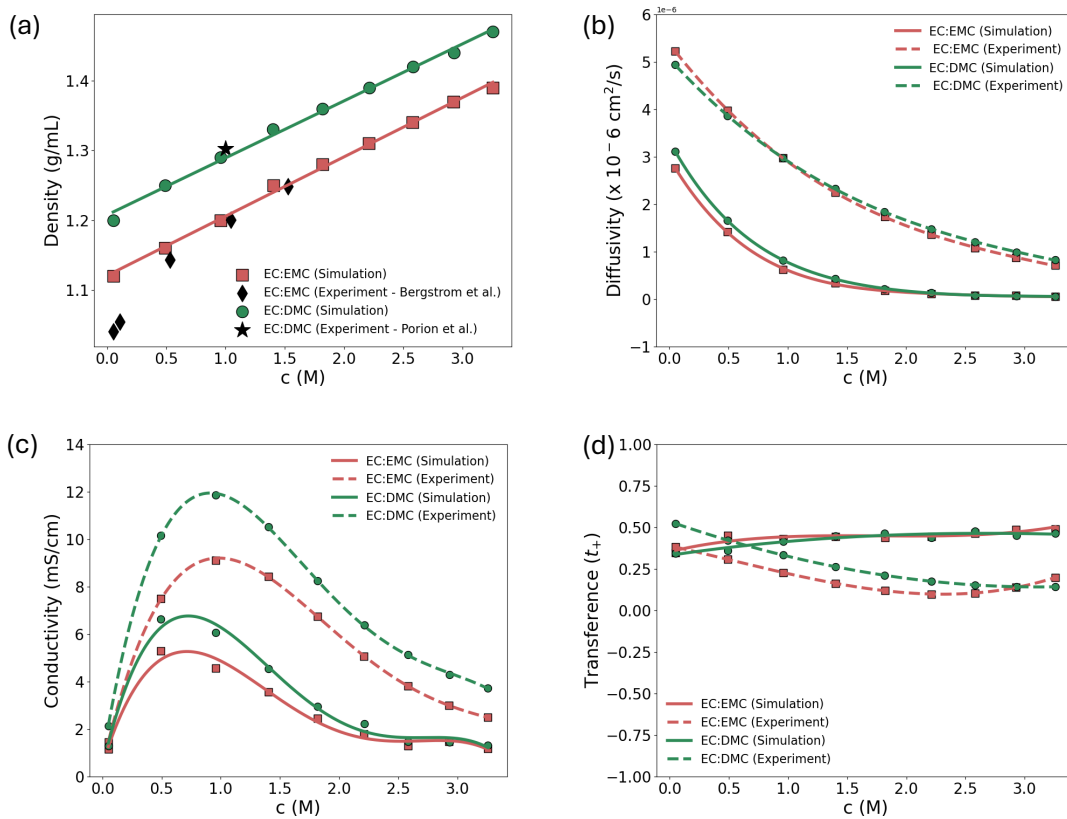


Figure 12: Simulation of transport properties of lithium ion battery liquid electrolytes, EC:EMC (3:7 w/w) and EC:DMC (1:1 w/w), at various molar concentrations (c) of LiPF_6 salt at 25°C . Panels (a-d) show the MD density, ionic diffusivity, ionic conductivity, and cationic transference number, respectively, which are obtained from MD simulation and compared with experimental results performed at 25°C . The experimental densities in (a) were taken from Refs. 119 and 120. The experimental results for diffusivity, conductivity and transference numbers in (b-d) were taken from Ref. 121

ture¹²⁵ were underestimated. However, even though the relative values of the ionic properties are underestimated in the simulations, the overall trends in the experimental property values between electrolyte formulations are accurately conserved within the MD simulations. Both experiment and simulation results demonstrate that both electrolyte formulations in our study have similar ionic diffusions. Nonetheless, the EC:DMC (1:1 w/w) mixture exhibited much higher ionic conductivity and cationic transference number than those of EC:EMC (3:7 w/w), due to its higher mass density.

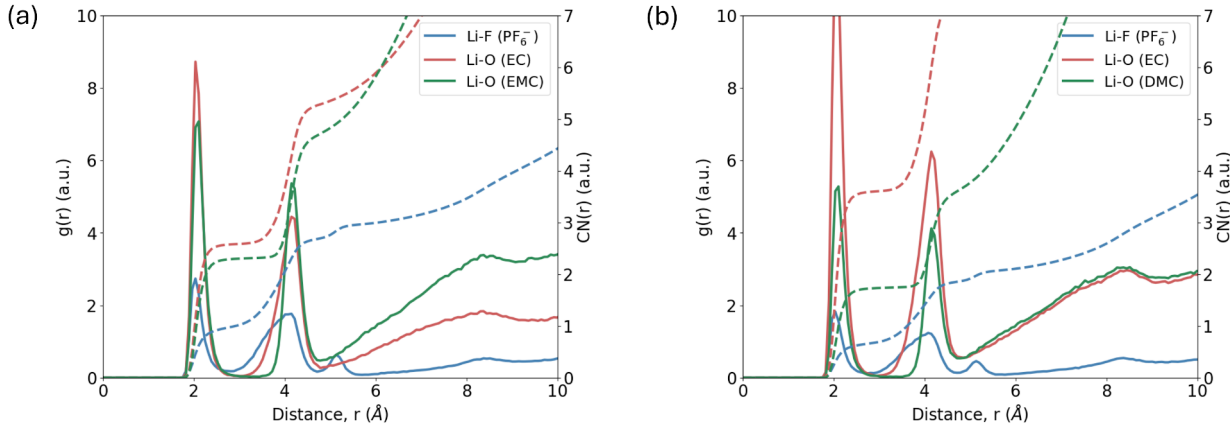


Figure 13: Calculated radial distribution function, $g(r)$, and corresponding coordination number integrals, $CN(r)$, of (a) Li-F (PF_6^-), Li-O (EC), Li-O (EMC) in EC:EMC (3:7 w/w) with 1M LiPF_6 , and (b) Li-F (PF_6^-), Li-O (EC), Li-O (DMC) in EC:DMC (1:1 w/w) with 1M LiPF_6

One of the key functionalities of SEAMM workflows is the ability to write custom python scripts within flowcharts, which enable on-the-fly post-processing of the MD simulation data. Figure 13 shows one such example where the radial distribution function, $g(r)$, and the corresponding coordination number, $CN(r)$, of solvated Li^+ ions in the above electrolyte formulations were calculated using a custom script that analyzed the MD trajectory data. In both formulations, we found that the first solvation shell is mostly occupied by the EC solvent molecules with a most probable distance of 2.05 Å to Li^+ , which is in agreement with previous MD studies of similar electrolyte systems.¹²⁶ The presence of EMC and DMC molecules within the first solvation shell depends on their relative ratios to the EC solvent

molecules. We found a substantial presence of EMC in EC:EMC (3:7 w/w) while the presence of DMC was almost half of EC in EC:DMC (1:1 w/w). The average Li^+ ion coordination number with solvent and salt is 5.84 for EC:EMC (3:7 w/w) and 5.98 for EC:DMC (1:1 w/w), which are also in good agreement with earlier MD studies.¹²⁶

Table 4: Thermal expansion in LiCoO_2

Lattice Constant	Expansion (K^{-1})
a	$8.36 \cdot 10^{-6}$
b	$8.36 \cdot 10^{-6}$
c	$2.04 \cdot 10^{-5}$
Average Expansion	$1.24 \cdot 10^{-5}$
Experimental Expansion	$1.30 \cdot 10^{-5}$

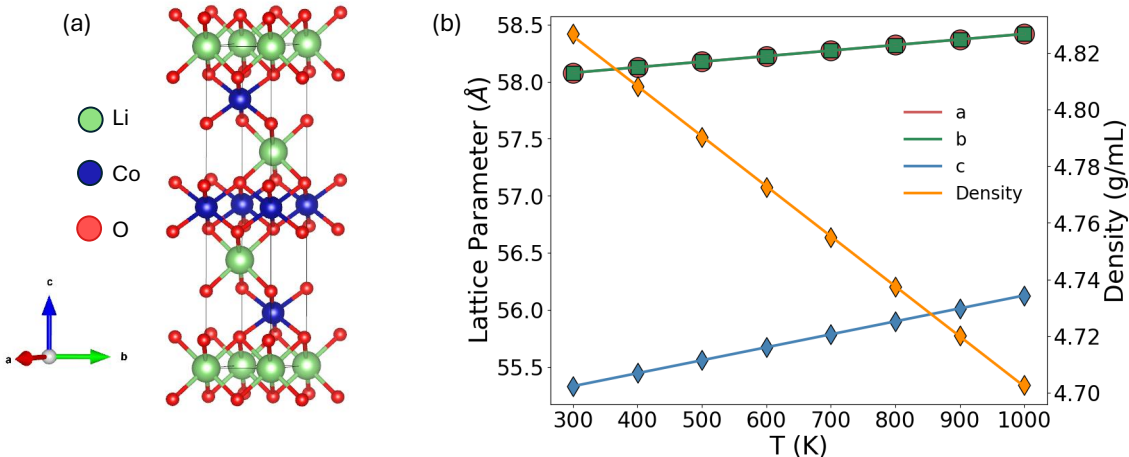


Figure 14: Thermal expansion in LiCoO_2 . (a) The experimental layered ($R3m$) crystal structure of LiCoO_2 used in the MD simulation. The Li, Co and O atoms are represented as green, blue and red spheres. (b) Lattice parameter expansion and change in density as a function of temperature in LiCoO_2 .

In the next part of our study, we focus on the prediction of the thermal expansion of LiCoO_2 at finite temperature using LAMMPS, as well as the simulation of thermal conductivity at various SOL at room temperature. We used SEAMM flowcharts for each step of the equilibrium MD simulations. Crystalline layered LiCoO_2 with rhombohedral symmetry (space group $R3m$, as shown in Figure 14(a)¹²⁷), and the Buckingham potential¹²⁸

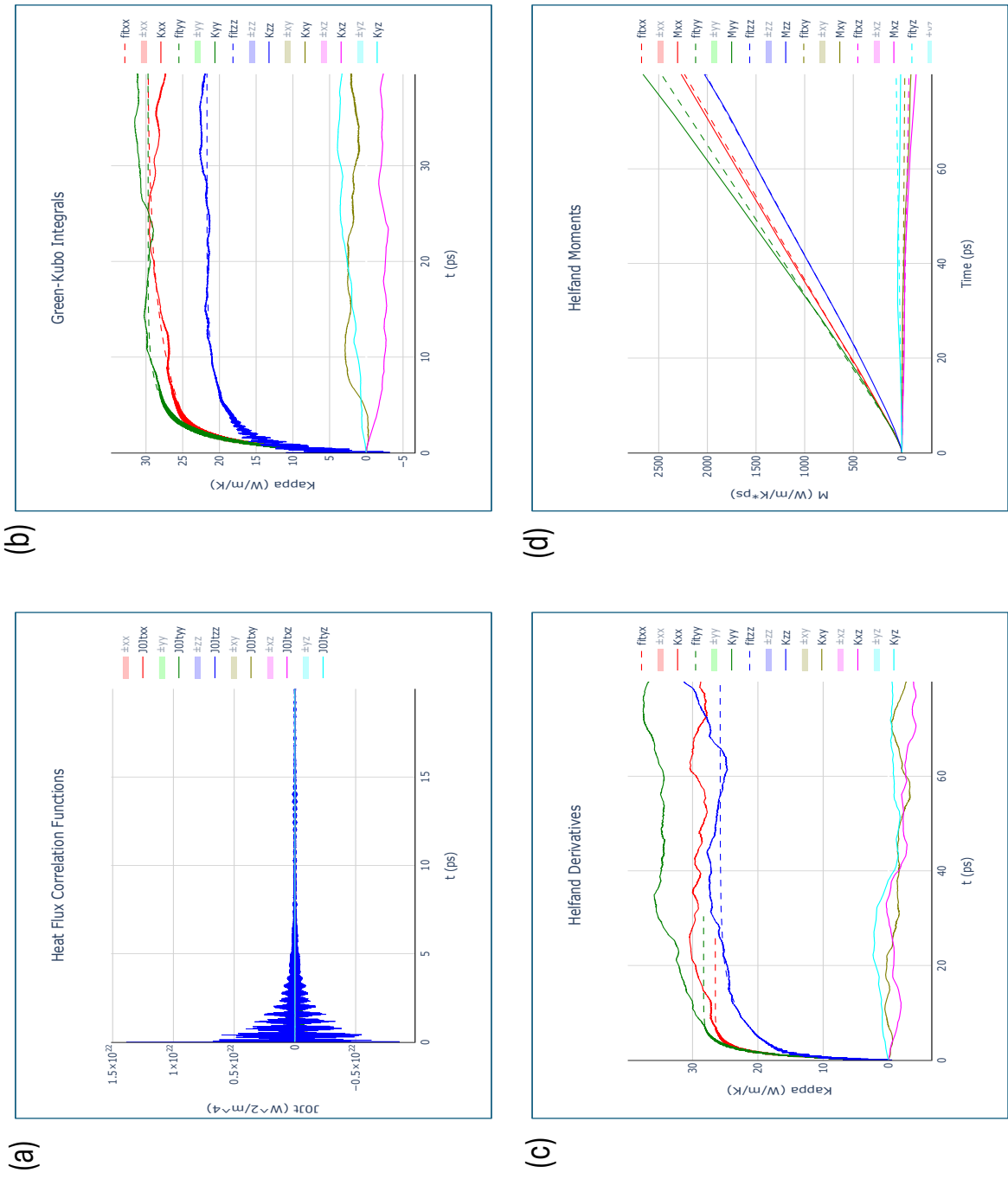


Figure 15: Thermal conductivity simulation of LiCoO₂ using equilibrium MD at $T = 298K$. Sample calculation of (a) heat flux auto-correlation function, (b) thermal conductivity fittings of Green-Kubo integrals, (c) thermal conductivity fitting of Helfand derivatives, and (d) Helfand moments as a function of time in ps.

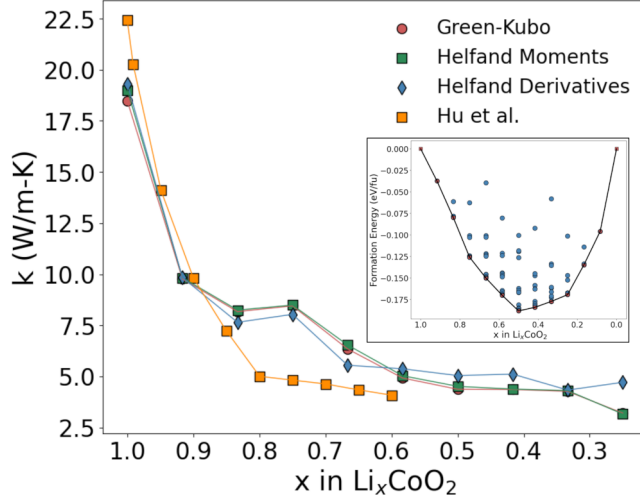


Figure 16: Calculated thermal conductivity of Li_xCoO_2 as a function of Li concentrations at $T = 298\text{K}$ from the MD simulation. The inset shows a convex hull diagram calculated using ab initio ground state formation energies to predict the lowest energy Li vacancy structures.

developed by Fisher *et al.*¹²⁹ were used for the simulations. The potential energy between pairs of ions in each crystalline solid was calculated by combining the long-range Coulombic component with a short range repulsive and attractive van der Waals interaction as described in Ref. 129. The short-range interactions, $\phi_{i,j}$, were described by a Buckingham potential of the form¹²⁹

$$\phi_{i,j}(r_{ij}) = A_{ij} \exp(-r_{ij}/\rho_{ij}) - C_{ij}/r_{ij}^6, \quad (5)$$

where, r_{ij} is the distance between the ions i and j , A_{ij} , ρ_{ij} and C_{ij} are parameters fit to experimental lattice parameters and ion positions as described in Ref. 129. A cutoff distance of 14 \AA was used for the Coulombic and Buckingham terms. First, equilibrium MD simulations with the isothermal-isobaric (NPT) ensemble were performed using a Nose-Hoover thermostat and barostat at a temperature T and a pressure of 1 atm for 200 ps, using a time step of 1 fs, to achieve thermal equilibration and to relax the structure. The lattice parameters of the relaxed geometry at each temperature T were then collected for the expansion calculation.

Figure 14(b) shows the in-plane and out-of-plane lattice parameters and the change in

mass density in LiCoO₂ as a function of temperature. The corresponding expansion coefficients (defined as $\Delta L/L\Delta T$, where L is the length of a lattice constant) along the lattice direction of a , b and c are shown in Table 4. The in-plane expansions are identical for the a and b directions and much smaller than the expansion along the out-of-plane c direction. This anisotropic lattice expansion is expected since the LiCoO₂ has a layered crystal structure where the Li and transition metal layers interact with each other with van der Waals interactions. The average thermal expansion coefficient predicted by the MD simulation ($1.24 \cdot 10^{-5} \text{ K}^{-1}$) is in close agreement with the experimental expansion coefficient from the polycrystalline LiCoO₂ pellets ($1.3 \cdot 10^{-5} \text{ K}^{-1}$).¹³⁰

Equilibrium MD methods such as Green-Kubo formalism,^{131,132} Helfand derivatives, and Helfand moments¹³³⁻¹³⁵ were used to predict the thermal conductivity of LiCoO₂. According to the Green-Kubo theory, which is derived from the fluctuation dissipation theorem and linear response theory, the thermal conductivity tensor $\kappa^{\alpha\beta}$ is proportional to the time integral of the heat flux autocorrelation function,^{131,132}

$$\kappa^{\alpha\beta}(T) = \frac{1}{k_B T^2 V} \int_0^\infty \langle J^\alpha(0) \cdot J^\beta(t) \rangle dt, \quad (6)$$

where, $J^\alpha(t)$ is the α th Cartesian component of the time-dependent heat current, k_B is the Boltzmann constant, V is the system volume, T is the system temperature, and $\langle \cdot \rangle$ denotes the ensemble average. In addition to the Green-Kubo approach, the Helfand moment and Helfand derivative approaches, which follow directly from the Green-Kubo expression,¹³³⁻¹³⁵ were used to calculate the thermal conductivity. The Helfand moment $G^\alpha(t)$ is defined in terms of the time integral of the heat current component J^α as

$$G^\alpha(t) = G^\alpha(0) + \int_0^t J^\alpha(\tau) d\tau \quad (7)$$

in which, the ensemble-averaged quantity, $M^{\alpha\beta}$, is defined as¹³⁴

$$M^{\alpha\beta}(t) = \langle (G^\alpha(t) - G^\alpha(0))(G^\beta(t) - G^\beta(0)) \rangle. \quad (8)$$

For a sufficiently long simulation time, $M^{\alpha\beta}(t)$ grows linearly as a function of time with a slope that is directly proportional to the corresponding thermal conductivity tensor component $\kappa^{\alpha\beta}(T)$.¹³⁶ Therefore, the thermal conductivity tensor $\kappa^{\alpha\beta}(T)$ is then defined in the Helfand approach as

$$\kappa^{\alpha\beta}(T) = \frac{1}{2tk_B T^2 V} \lim_{t \rightarrow \infty} M^{\alpha\beta}(t) \quad (9)$$

The advantage of the Helfand method over the more traditional Green-Kubo approach is two-fold. First, its convergence with simulation time is superior to that of Green-Kubo. Second, it is easier to fit the straight line given by Equation 9 than the exponential rise of the Green-Kubo function, which is complicated by the increasing noise as a function of time.

In order to calculate the time-dependent heat current autocorrelation function and apply it to the thermal conductivity calculation using the Green-Kubo and Helfand approaches, we performed production MD simulation with various run times. Before running the production runs, the system was further equilibrated for 200 ps, with a time step of 1 fs, of canonical (NVT) dynamics at a temperature T using a Nose-Hoover thermostat. Then simulations using the microcanonical (NVE) ensemble with a run length of 200 ps, 400 ps and 800 ps were carried out 10 times for each run length, for a total of 30 production runs, to calculate the heat flux autocorrelation function. The results of all the production runs were averaged to give the final thermal conductivity. Figure 15 shows a sample calculation of heat flux autocorrelation function, the Green-Kubo integrals, Helfand derivative, and Helfand moments for fully lithiated LiCoO_2 at $T = 300\text{K}$ for a 400 ps production run.

Figure 16 shows the calculated thermal conductivity of LiCoO_2 at various lithium concentrations at temperature of $T = 298\text{K}$. Each Li vacancy-ordered structure was first generated using DFT to calculate the formation energy of the convex hull of the ground state ($T = 0\text{K}$).

The inset in Figure 16 shows the convex hull diagram where the lowest energy structure was considered to be the most stable structure at any Li concentration x . Once these structures were identified, we used the classical MD simulation described above to calculate the thermal conductivity at $T = 298K$. All three approaches (Green-Kubo, Helfand moments, and Helfand derivatives) resulted in very similar thermal conductivities at any x considered in our calculations. Our results indicate that with the decrease in Li concentration during battery charging, the thermal conductivity decreases drastically from about 20 W/m/K at $x = 1$ to 3.2 W/m/K at $x = 0.3$. These results agree quantitatively with an earlier MD study by Hu *et al.*¹³⁷ where the nonequilibrium MD was used for the prediction of the thermal conductivity in LiCoO₂.

Conclusions

We have presented SEAMM, a new open source productivity tool and workflow environment for computational modeling and simulations of molecular and solid-state materials. SEAMM is underpinned by an extensive data model for molecular and crystalline structures implemented in an in-memory relational database using a traditional schema. The database also stores calculated properties and results by describing them with metadata using a star schema to connect the data to the metadata, allowing the data model to be modified and extended on the fly. This flexibility will permit SEAMM to adapt and change as current simulation tools evolve and new tools and methods are developed. An object-oriented facade is layered on top of the database, giving SEAMM a conventional data model from the software developers point of view. However, the flexibility and extensibility of the underlying model is carried through to the object-oriented model.

The heart of SEAMM are flowcharts, which represent simulation workflows in a graphical form. The functionality that users see in SEAMM is provided by independent software modules that plug-in to SEAMM and share data through the in-memory database. Each

plug-in corresponds to a step in a flowchart, presents its own graphical interface to users, implements the needed computation or simulation, and analyzes and presents the results. The only connection between plug-ins is the underlying data model in SEAMM. This decentralized approach allows any number of different groups to develop plug-ins with little or no coordination between groups. Users then create flowcharts to implement their workflows, combining plug-ins to do the simulations and modeling that are needed for their scientific or engineering problem.

There are a number of scriptable workflow tools for computational molecular and materials science (CMS), as well as a number of graphical tools for specific tasks. However, there is no general open source graphical workflow system for CMS. SEAMM fills this gap and extends the range of CMS tools. With a focus on productivity, on reducing the entry barrier to using a wide range of CMS simulation tools, and on the reproducibility and transparency of the workflows, SEAMM is a valuable contribution to the community.

Acknowledgement

The present work is funded by the National Science Foundation grants OAC-1547580 and CHE-2136142. PS and MM also acknowledge the Advanced Research Computing (<https://arc.vt.edu>) at Virginia Tech for providing computational resources and technical support that have contributed to the results reported within this manuscript.

References

- (1) Talirz, L.; Ghiringhelli, L. M.; Smit, B. Trends in Atomistic Simulation Software Usage. *Living Journal of Computational Molecular Science* **2021**, *3*, 1483.
- (2) Talirz, L.; Aprà, E.; Corsetti, F.; Moussa, J. E.; Poncé, S. Italirz/atomistic-software: v2024.3.29. 2024.

- (3) Haunschild, R.; Barth, A.; Marx, W. Evolution of DFT studies in view of a scientometric perspective. *Journal of Cheminformatics* **2016**, *8*, 1–12.
- (4) Dumaz, M.; Boucher, R.; Marques, M. A.; Romero, A. H. Authorship and citation cultural nature in density functional theory from solid state computational packages. *Scientometrics* **2021**, *126*, 6681–6695.
- (5) Bornmann, L.; Haunschild, R.; Mutz, R. Growth rates of modern science: a latent piecewise growth curve approach to model publication numbers from established and new literature databases. *Humanities and Social Sciences Communications* **2021**, *8*, 1–15.
- (6) Dongarra, J.; Meuer, M.; Simon, H.; Strohmaier, E. Computational capacity of the fastest supercomputers. <https://ourworldindata.org/grapher/supercomputer-power-flops>.
- (7) Pritchard, B. P.; Altarawy, D.; Didier, B.; Gibson, T. D.; Windus, T. L. New Basis Set Exchange: An Open, Up-to-Date Resource for the Molecular Sciences Community. *Journal of Chemical Information and Modeling* **2019**, *59*, 4814–4820, PMID: 31600445.
- (8) Simons, J. Why Is Quantum Chemistry So Complicated? *Journal of the American Chemical Society* **2023**, *145*, 4343–4354, PMID: 36787532.
- (9) Frisch, M. J. et al. Gaussian 03. Gaussian, Inc.: Wallingford, CT, 2004.
- (10) Frisch, M. J. et al. Gaussian 16 Revision C.01. 2016; Gaussian Inc. Wallingford CT.
- (11) Barca, G. M. J. et al. Recent developments in the general atomic and molecular electronic structure system. *The Journal of Chemical Physics* **2020**, *152*, 154102.
- (12) Kresse, G.; Hafner, J. Ab initio molecular dynamics for liquid metals. *Physical review B* **1993**, *47*, 558.

- (13) Kresse, G.; Hafner, J. Ab initio molecular-dynamics simulation of the liquid-metal–amorphous-semiconductor transition in germanium. *Physical Review B* **1994**, *49*, 14251.
- (14) Kresse, G.; Furthmüller, J. Efficiency of ab-initio total energy calculations for metals and semiconductors using a plane-wave basis set. *Computational materials science* **1996**, *6*, 15–50.
- (15) Kresse, G.; Furthmüller, J. Efficient iterative schemes for ab initio total-energy calculations using a plane-wave basis set. *Physical review B* **1996**, *54*, 11169.
- (16) Thompson, A. P.; Aktulga, H. M.; Berger, R.; Bolintineanu, D. S.; Brown, W. M.; Crozier, P. S.; In’t Veld, P. J.; Kohlmeyer, A.; Moore, S. G.; Nguyen, T. D., et al. LAMMPS—a flexible simulation tool for particle-based materials modeling at the atomic, meso, and continuum scales. *Computer Physics Communications* **2022**, *271*, 108171.
- (17) LAMMPS Documentation. <https://www.lammps.org>, Last Accessed: November 8, 2024.
- (18) Schappals, M.; Mecklenfeld, A.; Kröger, L.; Botan, V.; Köster, A.; Stephan, S.; García, E. J.; Rutkai, G.; Raabe, . G.; Klein, P.; Leonhard, K.; Glass, C. W.; Lenhard, J.; Vrabec, J.; Hasse, H. Round Robin Study: Molecular Simulation of Thermodynamic Properties from Models with Internal Degrees of Freedom. *Journal of Chemical Theory and Computation* **2017**, *13*, 4270–4280, PMID: 28738147.
- (19) Lehtola, S.; Steigemann, C.; Oliveira, M. J.; Marques, M. A. Recent developments in libxc—A comprehensive library of functionals for density functional theory. *SoftwareX* **2018**, *7*, 1–5.
- (20) Tadmor, E. B.; Elliott, R. S.; Sethna, J. P.; Miller, R. E.; Becker, C. A. The potential

- of atomistic simulations and the knowledgebase of interatomic models. *Jom* **2011**, *63*, 17.
- (21) OpenKIM: Interatomic Potentials and Analytics for Molecular Simulation. <https://openkim.org>, Last Accessed: February 10, 2025.
- (22) Jmol: an open-source Java viewer for chemical structures in 3D. <http://www.jmol.org/>, Last Accessed: November 11, 2024.
- (23) PyMol. <https://pymol.org>.
- (24) Sayle, R. A.; Milner-White, E. J. RASMOL: biomolecular graphics for all. *Trends in biochemical sciences* **1995**, *20*, 374–376.
- (25) VMD: Visual Molecular Dynamics. <http://www.ks.uiuc.edu/Research/vmd/>.
- (26) OVITO - Open Visualization Tool. <https://www.ovito.org>.
- (27) VESTA: Visualization for Electronic and STructural Analysis. <https://jp-minerals.org/vesta/en/>, Last Accessed: November 11, 2024.
- (28) CrystalMaker Software, Crystal/Molecular Structures Modelling & Diffraction. <https://crystalmaker.com>, Last Accessed: November 11, 2024.
- (29) Hanwell, M. D.; Curtis, D. E.; Lonie, D. C.; Vandermeersch, T.; Zurek, E.; Hutchison, G. R. Avogadro: an advanced semantic chemical editor, visualization, and analysis platform. *Journal of cheminformatics* **2012**, *4*, 1–17.
- (30) Avogadro: an open-source molecular builder and visualization tool. <http://avogadro.cc/>, Last Accessed: November 11, 2024.
- (31) Dennington, R.; Keith, T.; Millam, J. GaussView. <https://gaussian.com/gaussview6/>, Last Accessed: November 11, 2024.
- (32) Gabedit. <https://gabedit.sourceforge.net>, Last Accessed: November 11, 2024.

- (33) Allouche, A.-R. Gabedit—A graphical user interface for computational chemistry softwares. *Journal of Computational Chemistry* **2011**, *32*, 174–182.
- (34) Curtarolo, S.; Setyawan, W.; Hart, G. L.; Jahnatek, M.; Chepulskii, R. V.; Taylor, R. H.; Wang, S.; Xue, J.; Yang, K.; d Levy, O.; Mehl, M. J.; Stokes, H. T.; Demchenko, D. O.; Morgan, D. AFLOW: An automatic framework for high-throughput materials discovery. *Computational Materials Science* **2012**, *58*, 218–226.
- (35) Huber, S. P. et al. AiiDA 1.0, a scalable computational infrastructure for automated reproducible workflows and data provenance. *Scientific Data* **2020**, *7*, 300.
- (36) AiiDA: Automated workflows for computational science. <https://www.aiida.net>, Last Accessed: November 11, 2024.
- (37) Alegre-Requena, J. V.; Sowndarya SV, S.; Pérez-Soto, R.; Alturaifi, T. M.; Paton, R. S. AQME: Automated quantum mechanical environments for researchers and educators. *Wiley Interdisciplinary Reviews: Computational Molecular Science* **2023**, *13*, e1663.
- (38) Larsen, A. H. et al. The atomic simulation environment—a Python library for working with atoms. *Journal of Physics: Condensed Matter* **2017**, *29*, 273002.
- (39) Mathew, K.; Montoya, J. H.; Faghaninia, A.; Dwarakanath, S.; Aykol, M.; Tang, H.; Chu, I.-h.; Smidt, T.; Bocklund, B.; Horton, M., et al. Atomate: A high-level interface to generate, execute, and analyze computational materials science workflows. *Computational Materials Science* **2017**, *139*, 140–152.
- (40) Hicks, C. B.; Martinez, T. J. Massively scalable workflows for quantum chemistry: BigChem and ChemCloud. *The Journal of Chemical Physics* **2024**, *160*, 142501.
- (41) Lee, O. S.; Gather, M. C.; Zysman-Colman, E. Digichem: computational chemistry for everyone. *Digital Discovery* **2024**, *3*, 1695–1713.

- (42) Thompson, M. W.; Gilmer, J. B.; Matsumoto, R. A.; Quach, C. D.; Shamaprasad, P.; Yang, A. H.; Iacovella, C. R.; McCabe, C.; Cummings, P. T. Towards molecular simulations that are transparent, reproducible, usable by others, and extensible (TRUE). *Molecular Physics* **2020**, *118*, e1742938.
- (43) Janssen, J.; Surendralal, S.; Lysogorskiy, Y.; Todorova, M.; Hickel, T.; Drautz, R.; Neugebauer, J. pyiron: An integrated development environment for computational materials science. *Computational Materials Science* **2019**, *163*, 24–36.
- (44) Smith, D. G.; Altarawy, D.; Burns, L. A.; Welborn, M.; Naden, L. N.; Ward, L.; Ellis, S.; Pritchard, B. P.; Crawford, T. D. The MolSSI QCArchive project: An open-source platform to compute, organize, and share quantum chemistry data. *Wiley Interdisciplinary Reviews: Computational Molecular Science* **2021**, *11*, e1491.
- (45) Zapata, F.; Ridder, L.; Hidding, J.; Jacob, C. R.; Infante, I.; Visscher, L. QMflows: A Tool Kit for Interoperable Parallel Workflows in Quantum Chemistry. *Journal of Chemical Information and Modeling* **2019**, *59*, 3191–3197.
- (46) Gelžinytė, E.; Wengert, S.; Stenczel, T. K.; Heenen, H. H.; Reuter, K.; Csányi, G.; Bernstein, N. wfl Python toolkit for creating machine learning interatomic potentials and related atomistic simulation workflows. *The Journal of Chemical Physics* **2023**, *159*, 124801.
- (47) The Materials Project. <https://next-gen.materialsproject.org>, Last Accessed: February 10, 2025.
- (48) AFLOW: Automatic FLOW for Materials Discovery. <https://aflow.org>, Last Accessed: February 10, 2025.
- (49) MolSSI SEAMM: Simulation Environment for Atomistic and Molecular Modeling. <https://github.com/molssi-seamm>.

- (50) SEAMM: Simulation Environment for Atomistic and Molecular Modeling. <https://molssi-seamm.github.io>, Last Accessed: April 29, 2025.
- (51) Weininger, D. SMILES, a chemical language and information system. 1. Introduction to methodology and encoding rules. *Journal of Chemical Information and Computer Sciences* **1988**, *28*, 31–36.
- (52) National Center for Biotechnology Information. PubChem Compound Summary for CID 702, Ethanol. 2025; <https://pubchem.ncbi.nlm.nih.gov/compound/Ethanol>, Accessed on Feb. 11, 2025.
- (53) Jorgensen, W. L.; Tirado-Rives, J. Potential energy functions for atomic-level simulations of water and organic and biomolecular systems. *Proc. Natl. Acad. Sci. U. S. A.* **2005**, *102*, 6665–6670.
- (54) Nash, J.; Marin-Rimoldi, E.; Mostafanejad, M.; Saxe, P. SEAMM: Simulation Environment for Atomistic and Molecular Modeling. 2025; <https://doi.org/10.5281/zenodo.5153984>, Funding: NSF OAC-1547580 and CHE-2136142.
- (55) Marin-Rimoldi, E.; Saxe, P. LAMMPS plug-in for SEAMM. 2024; https://github.com/molssi-seamm/lammps_step, Last Accessed: November 11, 2024.
- (56) Saxe, P. PACKMOL plug-in for SEAMM. 2024; https://github.com/molssi-seamm/packmol_step, Last Accessed: November 11, 2024.
- (57) Shinoda, W.; Shiga, M.; Mikami, M. Rapid estimation of elastic constants by molecular dynamics simulation under constant stress. *Phys. Rev. B* **2004**, *69*, 134103.
- (58) Tuckerman, M. E.; Alejandre, J.; López-Rendón, R.; Jochim, A. L.; Martyna, G. J. A Liouville-operator derived measure-preserving integrator for molecular dynamics simulations in the isothermal–isobaric ensemble. *Journal of Physics A: Mathematical and General* **2006**, *39*, 5629.

- (59) Plimpton, S. Fast Parallel Algorithms for Short-Range Molecular Dynamics. *Journal of Computational Physics* **1995**, *117*, 1 – 19.
- (60) Dodda, L. S.; Cabeza de Vaca, I.; Tirado-Rives, J.; Jorgensen, W. L. LigParGen web server: an automatic OPLS-AA parameter generator for organic ligands. *Nucleic Acids Res.* **2017**, *45*, W331–W336.
- (61) Dodda, L. S.; Cabeza de Vaca, I.; Tirado-Rives, J.; Jorgensen, W. L. LigParGen generated parameters for CCO (ethanol). 2024; <https://traken.chem.yale.edu/ligpargen/>, Last Accessed: July 1 2024.
- (62) Dodda, L. S.; Vilseck, J. Z.; Tirado-Rives, J.; Jorgensen, W. L. 1.14*CM1A-LBCC: Localized bond-charge corrected CM1A charges for condensed-phase simulations. *J. Phys. Chem. B* **2017**, *121*, 3864–3870.
- (63) Hockney, R.; Eastwood, J. *Computer Simulation Using Particles*; Adam Hilger, 1988.
- (64) Sun, H. COMPASS: an ab initio force-field optimized for condensed-phase applications overview with details on alkane and benzene compounds. *The Journal of Physical Chemistry B* **1998**, *102*, 7338–7364.
- (65) Martínez, L.; Andrade, R.; Birgin, E. G.; Martínez, J. M. PACKMOL: A package for building initial configurations for molecular dynamics simulations. *Journal of Computational Chemistry* **2009**, *30*, 2157–2164.
- (66) Packmol - Creates Initial Configurations for Molecular Dynamics Simulations. 2024; <https://m3g.github.io/packmol>, Last Accessed: August 1, 2024.
- (67) O’Boyle, N. M.; Banck, M.; James, C. A.; Morley, C.; Vandermeersch, T.; Hutchison, G. R. Open Babel: An open chemical toolbox. *Journal of Cheminformatics* **2011**, *3*, 33.

- (68) The Open Babel Package. 2023; <http://openbabel.org>, Last Accessed: November 1, 2024.
- (69) Python implementation of the multistate Bennett acceptance ratio (MBAR) method. 2023; <https://github.com/choderalab/pymbar>, Last Accessed: August 1, 2024.
- (70) Chodera, J. D. A Simple Method for Automated Equilibration Detection in Molecular Simulations. *Journal of Chemical Theory and Computation* **2016**, *12*, 1799–1805, PMID: 26771390.
- (71) Shirts, M. R.; Chodera, J. D. Statistically optimal analysis of samples from multiple equilibrium states. *The Journal of Chemical Physics* **2008**, *129*, 124105.
- (72) Chodera, J. D.; Swope, W. C.; Pitera, J. W.; Seok, C.; Dill, K. A. Use of the Weighted Histogram Analysis Method for the Analysis of Simulated and Parallel Tempering Simulations. *Journal of Chemical Theory and Computation* **2007**, *3*, 26–41, PMID: 26627148.
- (73) Python Package Index - PyPI. <https://pypi.org/>, Last Accessed: July 11, 2024.
- (74) Thermodynamic system. https://en.wikipedia.org/wiki/Thermodynamic_system, Last Accessed: April 29, 2025.
- (75) SQLite. <https://www.sqlite.org>, Last Accessed: April 29, 2025.
- (76) Star schema. https://en.wikipedia.org/wiki/Star_schema, Last Accessed: April 29, 2025.
- (77) Pint: makes units easy. <https://github.com/hgrecco/pint>, Last Accessed: April 29, 2025.
- (78) O’Boyle, N. M.; Banck, M.; James, C. A.; Morley, C.; Vandermeersch, T.; Hutchison, G. R. Open Babel: An open chemical toolbox. *Journal of Cheminformatics* **2011**, *3*, 33.

- (79) RDKit: Open-source cheminformatics. <https://www.rdkit.org>, Last Accessed: April 29, 2025.
- (80) Wang, L.-P.; Song, C. Geometry optimization made simple with translation and rotation coordinates. *The Journal of Chemical Physics* **2016**, *144*, 214108.
- (81) tkinter — Python interface to Tcl/Tk. <https://docs.python.org/3/library/tkinter.html>, Last Accessed: April 29, 2025.
- (82) Saxe, P. SEAMM Cookiecutter. <https://github.com/molssi-seamm/seamm-cookiecutter>, Last Accessed: November 11, 2024.
- (83) Naden, L. N.; Nash, J. A. Cookiecutter for Computational Molecular Sciences (CMS) Python Packages. <https://github.com/MolSSI/cookiecutter-cms>, Last Accessed: November 11, 2024.
- (84) European Organization For Nuclear Research,; OpenAIRE, Zenodo. 2013; <https://www.zenodo.org/>.
- (85) Liskow, D. H.; Bender, C. F.; Schaefer, I., Henry F. Some Features of the CH₃NC→CH₃CN Potential Surface. *The Journal of Chemical Physics* **1972**, *57*, 4509–4511.
- (86) Liskow, D. H.; Bender, C. F.; Schaefer, H. F. I. Theoretical reaction coordinate for the methyl isocyanide isomerization. *Journal of the American Chemical Society* **1972**, *94*, 5178–5182.
- (87) Redmon, L. T.; Purvis, G. D.; Bartlett, R. J. The unimolecular isomerization of methyl isocyanide to methyl cyanide (acetonitrile). *The Journal of Chemical Physics* **1978**, *69*, 5386–5392.
- (88) Saxe, P.; Yamaguchi, Y.; Pulay, P.; Schaefer, H. F. Transition state vibrational analysis

- for the methyl isocyanide rearrangement, CH₃NC → CH₃CN. *Journal of the American Chemical Society* **1980**, *102*, 3718 – 3723.
- (89) Nguyen, T. L.; Thorpe, J. H.; Bross, D. H.; Ruscic, B.; Stanton, J. F. Unimolecular Reaction of Methyl Isocyanide to Acetonitrile: A High-Level Theoretical Study. *The Journal of Physical Chemistry Letters* **2018**, *9*, 2532–2538, PMID: 29697985.
- (90) Smith, D. G. A. et al. PSI4 1.4: Open-source software for high-throughput quantum chemistry. *The Journal of Chemical Physics* **2020**, *152*, 184108.
- (91) Jónsson, H.; Mills, G.; Jacobsen, K. W. *Classical and Quantum Dynamics in Condensed Phase Simulations*; pp 385–404.
- (92) Henkelman, G.; Jónsson, H. Improved tangent estimate in the nudged elastic band method for finding minimum energy paths and saddle points. *The Journal of Chemical Physics* **2000**, *113*, 9978–9985.
- (93) Makri, S.; Ortner, C.; Kermode, J. R. A preconditioning scheme for minimum energy path finding methods. *The Journal of Chemical Physics* **2019**, *150*, 094109.
- (94) Henkelman, G.; Uberuaga, B. P.; Jónsson, H. A climbing image nudged elastic band method for finding saddle points and minimum energy paths. *The Journal of Chemical Physics* **2000**, *113*, 9901–9904.
- (95) Smidstrup, S.; Pedersen, A.; Stokbro, K.; Jónsson, H. Improved initial guess for minimum energy path calculations. *The Journal of Chemical Physics* **2014**, *140*, 214106.
- (96) Blum, V.; Gehrke, R.; Hanke, F.; Havu, P.; Havu, V.; Ren, X.; Reuter, K.; Scheffler, M. Ab initio molecular simulations with numeric atom-centered orbitals. *Computer Physics Communications* **2009**, *180*, 2175–2196.
- (97) Havu, V.; Blum, V.; Havu, P.; Scheffler, M. Efficient O(N) integration for all-electron

- electronic structure calculation using numeric basis functions. *Journal of Computational Physics* **2009**, *228*, 8367–8379.
- (98) Zhang, I. Y.; Ren, X.; Rinke, P.; Blum, V.; Scheffler, M. Numeric atom-centered-orbital basis sets with valence-correlation consistency from H to Ar. *New Journal of Physics* **2013**, *15*, 123033.
- (99) Stewart, J. J. P.; Klamt, A.; Thiel, W.; Danovich, D.; Rocha, G. B.; Giesecking, R. L.; Moussa, J. E.; Kurtz, H. A.; Korambath, P.; Merz, K. M.; Wang, B. MOPAC. 2022; <https://doi.org/10.5281/zenodo.6811510>, If you use this software for a scientific publication, please cite it as below.
- (100) Stewart, J. J.; Stewart, A. C. A semiempirical method optimized for modeling proteins. *Journal of Molecular Modeling* **2023**, *29*, 284.
- (101) Stewart, J. J. P. Optimization of parameters for semiempirical methods VI: more modifications to the NDDO approximations and re-optimization of parameters. *Journal of Molecular Modeling* **2012**, *19*, 1–32.
- (102) Elstner, M.; Porezag, D.; Jungnickel, G.; Elsner, J.; Haugk, M.; Frauenheim, T.; Suhai, S.; Seifert, G. Self-consistent-charge density-functional tight-binding method for simulations of complex materials properties. *Physical Review B* **1998**, *58*, 7260.
- (103) Hourahine, B. et al. DFTB+, a software package for efficient approximate density functional theory based atomistic simulations. *The Journal of Chemical Physics* **2020**, *152*, 124101.
- (104) Gaus, M.; Goez, A.; Elstner, M. Parametrization and Benchmark of DFTB3 for Organic Molecules. *Journal of Chemical Theory and Computation* **2013**, *9*, 338–354, PMID: 26589037.

- (105) Bannwarth, C.; Caldeweyher, E.; Ehlert, S.; Hansen, A.; Pracht, P.; Seibert, J.; Spicher, S.; Grimme, S. Extended tight-binding quantum chemistry methods. *WIREs Computational Molecular Science* **2021**, *11*, e1493.
- (106) Bannwarth, C.; Ehlert, S.; Grimme, S. GFN2-xTB—An Accurate and Broadly Parametrized Self-Consistent Tight-Binding Quantum Chemical Method with Multipole Electrostatics and Density-Dependent Dispersion Contributions. *Journal of Chemical Theory and Computation* **2019**, *15*, 1652–1671, PMID: 30741547.
- (107) Strachan, A.; van Duin, A. C. T.; Chakraborty, D.; Dasgupta, S.; Goddard, W. A. Shock Waves in High-Energy Materials: The Initial Chemical Events in Nitramine RDX. *Phys. Rev. Lett.* **2003**, *91*, 098301.
- (108) Singh, S. K.; Srinivasan, S. G.; Neek-Amal, M.; Costamagna, S.; van Duin, A. C. T.; Peeters, F. M. Thermal properties of fluorinated graphene. *Phys. Rev. B* **2013**, *87*, 104114.
- (109) Shan, T.-R.; Wixom, R. R.; Thompson, A. P. *Nanoscale Void-Enhanced Initiation in Hexanitrostilbene: Reactive Molecular Dynamics Simulations.*; 2014.
- (110) Smith, J. S.; Nebgen, B. T.; Zubatyuk, R.; Lubbers, N.; Devereux, C.; Barros, K.; Tretiak, S.; Isayev, O.; Roitberg, A. E. Approaching coupled cluster accuracy with a general-purpose neural network potential through transfer learning. *Nature Communications* **2019**, *10*, 2903.
- (111) Devereux, C.; Smith, J. S.; Huddleston, K. K.; Barros, K.; Zubatyuk, R.; Isayev, O.; Roitberg, A. E. Extending the Applicability of the ANI Deep Learning Molecular Potential to Sulfur and Halogens. *Journal of Chemical Theory and Computation* **2020**, *16*, 4192–4202, PMID: 32543858.
- (112) Jorgensen, W. L.; Maxwell, D. S.; Tirado-Rives, J. Development and testing of the

- OPLS all-atom force field on conformational energetics and properties of organic liquids. *Journal of the American Chemical Society* **1996**, *118*, 11225–11236.
- (113) Kaminski, G. A.; Friesner, R. A.; Tirado-Rives, J.; Jorgensen, W. L. Evaluation and reparametrization of the OPLS-AA force field for proteins via comparison with accurate quantum chemical calculations on peptides. *The Journal of Physical Chemistry B* **2001**, *105*, 6474–6487.
- (114) Jensen, K. P.; Jorgensen, W. L. Halide, ammonium, and alkali metal ion parameters for modeling aqueous solutions. *Journal of Chemical Theory and Computation* **2006**, *2*, 1499–1509.
- (115) Canongia Lopes, J. N.; Pádua, A. A. Molecular force field for ionic liquids composed of triflate or bistriflylimide anions. *The Journal of Physical Chemistry B* **2004**, *108*, 16893–16898.
- (116) Bizeray, A. M.; Howey, D. A.; Monroe, C. W. Resolving a discrepancy in diffusion potentials, with a case study for Li-ion batteries. *Journal of The Electrochemical Society* **2016**, *163*, E223.
- (117) France-Lanord, A.; Grossman, J. C. Correlations from ion pairing and the Nernst-Einstein equation. *Physical review letters* **2019**, *122*, 136001.
- (118) Pesko, D. M.; Timachova, K.; Bhattacharya, R.; Smith, M. C.; Villaluenga, I.; Newman, J.; Balsara, N. P. Negative transference numbers in poly (ethylene oxide)-based electrolytes. *Journal of The Electrochemical Society* **2017**, *164*, E3569.
- (119) Bergstrom, H. K.; Fong, K. D.; McCloskey, B. D. Interfacial effects on transport coefficient measurements in Li-ion battery electrolytes. *Journal of The Electrochemical Society* **2021**, *168*, 060543.

- (120) Porion, P.; Dougassa, Y. R.; Tessier, C.; El Ouatani, L.; Jacquemin, J.; Anouti, M. Comparative study on transport properties for LiFAP and LiPF₆ in alkyl-carbonates as electrolytes through conductivity, viscosity and NMR self-diffusion measurements. *Electrochimica Acta* **2013**, *114*, 95–104.
- (121) Landesfeind, J.; Gasteiger, H. A. Temperature and concentration dependence of the ionic transport properties of lithium-ion battery electrolytes. *Journal of The Electrochemical Society* **2019**, *166*, A3079–A3097.
- (122) Zhou, J.; He, H.; Xing, F.; Long, Y.; Mo, T. Optimization of the OPLS force field for "water-in-salt" electrolytes. *Journal of Molecular Liquids* **2024**, *403*, 124923.
- (123) Ruza, J.; Leon, P.; Jun, K.; Johnson, J.; Shao-Horn, Y.; Gómez-Bombarelli, R. Benchmarking Classical Molecular Dynamics Simulations for Computational Screening of Lithium Polymer Electrolytes. **2025**,
- (124) Lu, C.; Wu, C.; Ghoreishi, D.; Chen, W.; Wang, L.; Damm, W.; Ross, G. A.; Dahlgren, M. K.; Russell, E.; Von Bargen, C. D., et al. OPLS4: Improving force field accuracy on challenging regimes of chemical space. *Journal of chemical theory and computation* **2021**, *17*, 4291–4300.
- (125) Dajnowicz, S.; Agarwal, G.; Stevenson, J. M.; Jacobson, L. D.; Ramezanghorbani, F.; Leswing, K.; Friesner, R. A.; Halls, M. D.; Abel, R. High-dimensional neural network potential for liquid electrolyte simulations. *The Journal of Physical Chemistry B* **2022**, *126*, 6271–6280.
- (126) Hou, T.; Yang, G.; Rajput, N. N.; Self, J.; Park, S.-W.; Nanda, J.; Persson, K. A. The influence of FEC on the solvation structure and reduction reaction of LiPF₆/EC electrolytes and its implication for solid electrolyte interphase formation. *Nano Energy* **2019**, *64*, 103881.

- (127) Rodriguez, M. A.; Ingersoll, D.; Doughty, D. H. Quantitative analysis of Li contents in Li_xCoO_2 cathodes via Rietveld refinement. *Powder Diffraction* **2003**, *18*, 135–139.
- (128) Buckingham, R. A. The classical equation of state of gaseous helium, neon and argon. *Proceedings of the Royal Society of London. Series A. Mathematical and Physical Sciences* **1938**, *168*, 264–283.
- (129) AJ Fisher, C.; Saiful Islam, M.; Moriwake, H. Atomic level investigations of lithium ion battery cathode materials. *Journal of the Physical Society of Japan* **2010**, *79*, 59–64.
- (130) Cheng, E. J.; Taylor, N. J.; Wolfenstine, J.; Sakamoto, J. Elastic properties of lithium cobalt oxide (LiCoO_2). *Journal of Asian Ceramic Societies* **2017**, *5*, 113–117.
- (131) Green, M. S. Markoff random processes and the statistical mechanics of time-dependent phenomena. II. Irreversible processes in fluids. *The Journal of chemical physics* **1954**, *22*, 398–413.
- (132) Kubo, R.; Yokota, M.; Nakajima, S. Statistical-mechanical theory of irreversible processes. II. Response to thermal disturbance. *Journal of the Physical Society of Japan* **1957**, *12*, 1203–1211.
- (133) Helfand, E. Transport coefficients from dissipation in a canonical ensemble. *Physical Review* **1960**, *119*, 1.
- (134) Gaspard, P. Chaos, scattering and statistical mechanics. *Chaos* **2005**,
- (135) Viscardy, S.; Servantie, J.; Gaspard, P. Transport and Helfand moments in the Lennard-Jones fluid. I. Shear viscosity. *The Journal of chemical physics* **2007**, *126*.
- (136) Pereverzev, A.; Sewell, T. Heat-current filtering for Green–Kubo and Helfand-moment molecular dynamics predictions of thermal conductivity: Application to the organic crystal β -HMX. *International Journal of Heat and Mass Transfer* **2022**, *188*, 122647.

- (137) Hu, S.; Zhang, Z.; Wang, Z.; Zeng, K.; Cheng, Y.; Chen, J.; Zhang, G. Significant reduction in thermal conductivity of lithium cobalt oxide cathode upon charging: propagating and non-propagating thermal energy transport. *ES Energy & Environment* **2018**, *1*, 74–79.

Supporting Information:

SEAMM: A Simulation Environment for Atomistic and Molecular Modeling

Paul Saxe,^{*,†,‡} Jessica Nash,^{*,†,‡} Mohammad Mostafanejad,^{*,†,‡} Eliseo
Marin-Rimoldi,^{*,¶} Hasnain Hafiz,^{*,§} Louis G Hector, Jr.,^{*,§} and T. Daniel
Crawford^{*,†,‡}

[†]*Department of Chemistry, Virginia Tech, Blacksburg, Virginia 24061, USA*

[‡]*Molecular Sciences Software Institute, Blacksburg, Virginia 24060, USA*

[¶]*Department of Chemical and Biomolecular Engineering, University of Notre Dame, Notre
Dame, Indiana 46556, USA*

[§]*Battery Research and Development, General Motors, Warren, MI 48092, USA*

E-mail: psaxe@vt.edu; janash@vt.edu; smostafanejad@vt.edu; emarinri@nd.edu;
hasnain.hafiz@gm.com; louis.hector@gm.com; crawdad@vt.edu

Contents

Introduction	3
Flowchart for Reaction Paths	3
Initialization	5
Optimization of the Reactant and Product Structures	6
The Reaction Path and Approximate Transition States	7
Optimization of the Key Structures and Their Thermochemistry	8
Reaction Path for the Rearrangement of Methylisocyanide to Isonitrile	11

Introduction

This supplementary material covers the simulations and results of Example 2 in the paper in more detail. The first part describes the calculations underlying Tables 1 and 2. The second part covers the calculations with ReaxFF and TorchaANI, expanding on the results mentioned in the paper and some exploration of the nature of the potential energy surface for these methods.

Flowchart for Reaction Paths

Finding the transition state for a reaction and calculating the energies and enthalpies of the reactants, transition state, and products requires a number of distinct calculations:

1. Determining the structures of the reactant(s) and product(s);
2. Locating the transition state between the reactants(s) and product(s);
3. Refining the structure of the transition state;
4. Calculating the thermochemical functions in the harmonic approximation for the reactant(s), transition state, and product(s)

Each of these parts can be handled with a separate flowchart in Simulation Environment for Atomistic and Molecular Modeling (SEAMM), or two or more parts can be combined in a single flowchart. Figure 1 shows a single flowchart for handling all the needed calculations, which is convenient for running either many different methods for a single reaction, or investigating many reactions.

This flowchart corresponds directly to the steps above, as shown by the green text boxes. The next subsections describe the flowchart in some detail because it nicely illustrates the flexibility and power of SEAMM. However, since the flowchart implements a reasonably

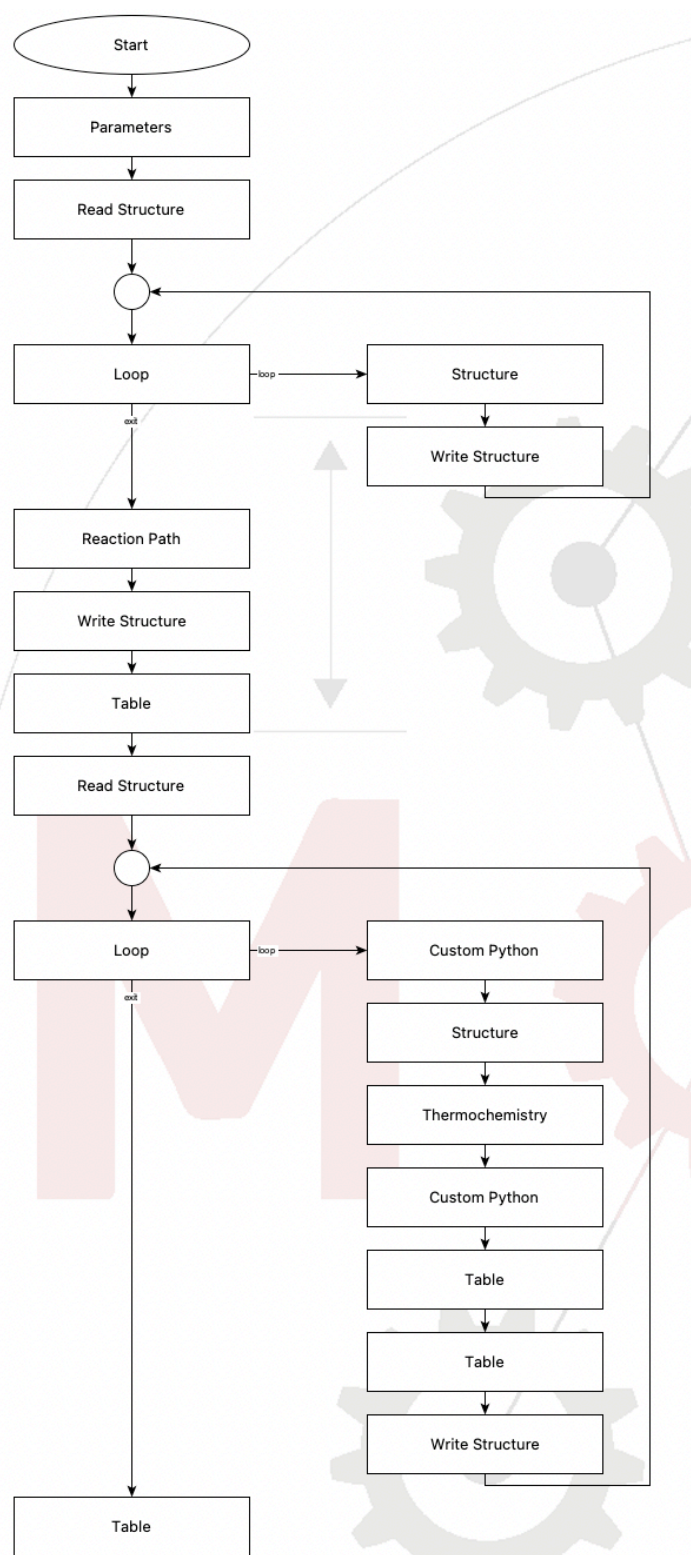


Figure 1: Flowchart for Reaction Thermochemistry

complicated workflow, the description is quite lengthy, and may be skipped if the detail is not of interest.

This flowchart uses loops to handle the initial structures as well as the final structures, **Table** steps to capture and tabulate the key results, and **Custom Python** steps to customize small parts of the flowchart. These steps will be covered in more detail below.

Initialization

It starts with a **Parameters** step that defines the value of variables that control parts of the flowchart. As mentioned, this makes the flowchart more general because the user can set the parameters when submitting the job, rather than edit the flowchart. Figure 2 shows the dialog for editing the control parameters.

Edit Parameters										
	Name	Type	NArgs	Optional	Overwrite?	Default	Help			
-	Edit	structure	file	a single value	Yes	No	/Users/psaxe/Dropbox/SEAMM_Paper/structures/CH3NC-CH3CN.sdf	The structure file for the reactant/product		
-	Edit	reactant	str	a single value	Yes	No	reaction/methylisocyanide	system/configuration of the reactant		
-	Edit	product	str	a single value	Yes	No	reaction/methylcyanide	system/configuration of the product		
-	Edit	n_intermediates	int	a single value	Yes	No	3	Number of intermediate structures in the path (>= 3)		
-	Edit	climb	bool	a single value	Yes	No		Whether to use a climbing image at the end		
-	Edit	interpolation	str	a single value	Yes	No	Image Dependent Pair Potential (IDPP)	How to interpolate the path		
-	Edit	convergence	float	a single value	Yes	No	100	The force convergence in kJ/mol/Å		
-	Edit	nsteps	str	a single value	Yes	No	300	Number of steps of NEB		
-	Edit	spring	float	a single value	Yes	No	1000	The spring constant in NEB		
-	Edit	remove	str	a single value	Yes	No	once before starting	Whether to remove rotations and translations		
-	Edit	hamiltonian	str	a single value	Yes	No	PM6-org	The parameterization or method for the calculation		
+										

Figure 2: Control parameters for the reaction path flowchart

The first three parameters define the reactants and products for the reaction by giving the file containing the structures — in this case an structure-data format (SDF) file — and the names of the structures in that file that are the reactants and products. The assumption is that these structures have been prepared and placed in a file, which gives considerable flexibility in defining the reactant and product systems. Using these variables to define the reactants and products makes the flowchart general and applicable to many different reactions.

The next group of parameters control the nudged elastic band (NEB) method¹⁻³ used to find an approximate transition state. The NEB employs a number of structures between the reactants and products connected from the reactants through the intermediate structures to the products with an elastic band. *n_intermediates* defines how many structures to use between the reactants and products, while *spring* gives the force constant for the elastic bands between adjacent structures. *interpolation* determines the initial guess for the intermediate structures, which can currently be linear interpolation or the image dependent pair potential (IDPP)⁴ method. *climb* controls whether to use the standard NEB method or climbing image nudged elastic band (CI-NEB)⁵ where the highest energy image is allowed to climb upwards towards the transition state, rather than remaining roughly in the middle between its two adjacent intermediate structures. *remove* controls whether to remove rigid rotations and translations and rotations between the various structures, and if so whether to do so just at the beginning of the calculation or at each step. Finally, *convergence* and *nsteps* give the convergence criterion for the calculation and a maximum number of steps before giving up if the calculation does not converge.

The last parameter, *hamiltonian*, specifies the parametrization for semiempirical methods, or the method for textitab initio methods, or the forcefield for molecular mechanics. This allows the flowchart to be used for a variety of different approaches without editing. This parameter is used in the all the steps from the initial structure optimization through the reaction path to the final structure optimization and thermochemistry calculation.

Together, these parameters give considerable flexibility in defining the calculations in the flowchart, allowing the user to tune the calculation to their needs.

Optimization of the Reactant and Product Structures

After reading the structure file, the flowchart continues with a loop over the structures in the file, which are then optimized using the **Structure** step, which wraps the open source code **geomeTRIC**⁶ to handle the structural optimization. As has been mentioned, the **Structure**,

as well as the `Reaction Path`, and `Thermochemistry` steps rely on a subflowchart to calculate the energy and forces for the structure, as shown in Figure 3, which uses DFTB+ for the energy and forces.

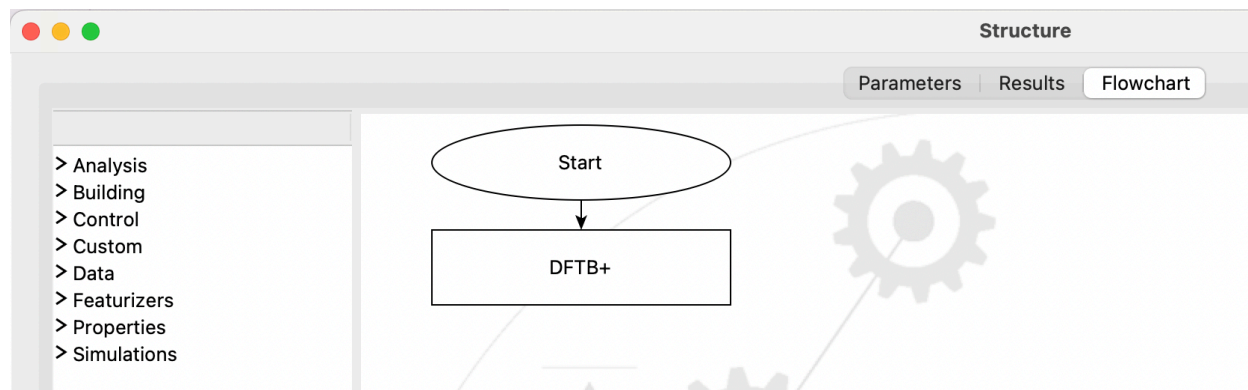


Figure 3: An example of the subflowchart common to the `Structure`, `Reaction Path`, `Thermochemistry`, and `Energy Scan` steps.

The flowchart to calculate the energy and forces using DFTB+ shown in Figure 4 is straightforward. Using any other simulation code to calculate the energy and forces is similarly simple, making it easy to switch between codes.

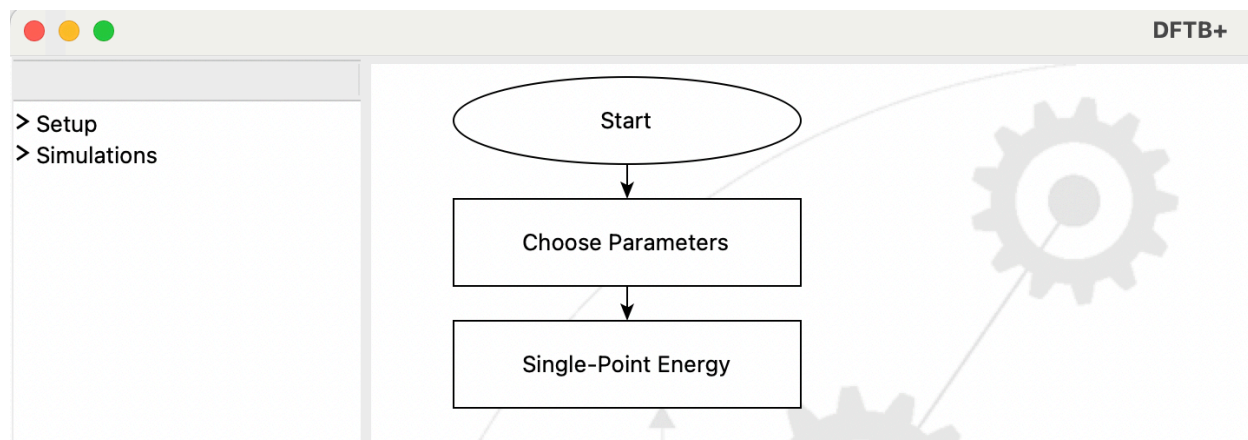


Figure 4: The flowchart to calculate the energy and forces using DFTB+.

The Reaction Path and Approximate Transition States

Once the structures for the reactants and products are optimized, the flowchart moves to the `Reaction Path` step, which uses the NEB and CI-NEB methods as implemented in

Atomic Simulation Environment (ASE)⁷ to find and approximate reaction path and transition state. The **Reaction Path** step uses an identical subflowchart to that shown above for the **Structure** step. Indeed, SEAMM supports copying and pasting flowcharts so the subflowchart can simply be copied from the **Structure** step. As noted above, several parameters controlling the NEB algorithm are defined by the initial **Parameters** step as variables, giving considerable flexibility in how to approach the NEB calculation.

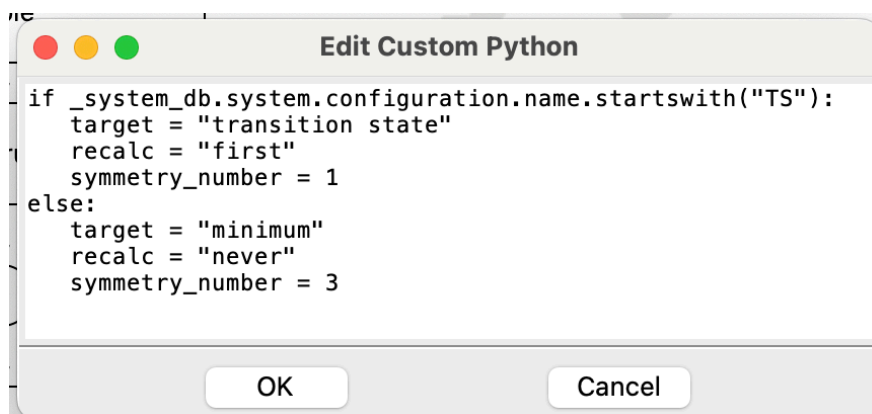
As the steps in the flowchart run, the various structures that are generated are stored in the internal database in SEAMM for later use. In this flowchart the **Write Structure** step immediately after the **Reaction Path** step writes an SDF file with all the structures along the reaction path from the NEB calculation so that they can be viewed or used later. After creating a table with the **Table** step, which will be discussed a bit later, the flowchart proceeds to reading the structures for the stationary points that the **Reaction Path** step found and wrote to a specific SDF file. Note that while we have been talking as if there is a single transition state in the reaction path, that is the reaction is an elementary reaction, the NEB method is capable of handling more complex reactions with multiple transition states and intermediate structures between them. In such cases, all the stationary point structures would be output from the **Reaction Path** step and used in the subsequent steps of the flowchart.

Optimization of the Key Structures and Their Thermochemistry

The final **loop** step in the flow chart handles the optimization of the structures of the stationary points along the reaction path. If the reaction is an elementary reaction with just one transition state, there will be three structures: the reactants, the transition state, and the products. For more complicated reactions, there would be additional transition states as well as intermediate minima between them. In all cases, the loop optimizes each structure in the **Structure** step, calculating the thermochemical functions for each structure in the **Thermochemistry** step, which uses the identical subflowchart to the initial **Structure** step,

which can be copied and pasted into this step. Internally the **Thermochemistry** is using the `thermochemistry` module from ASE⁷ to calculate the harmonic approximation to the thermochemical functions of the vibrational frequencies.

There is a small issue with the optimizer that the **Custom Step** at the beginning of the loop solves. The optimizer in the **Structure** step needs to know whether it is targeting a minimum or a transition state. At the moment, the **Thermochemistry** step requires the symmetry number for the structure. In a future release, the **Thermochemistry** step will be enhanced to automatically determine the symmetry number, but for the moment it needs to be set manually or using a variable as shown in Figure 5.



```
if _system_db.system.configuration.name.startswith("TS"):
    target = "transition state"
    recalc = "first"
    symmetry_number = 1
else:
    target = "minimum"
    recalc = "never"
    symmetry_number = 3
```

Figure 5: The Python code to set the required parameters for the **Structure** and **Thermochemistry** steps.

The somewhat cryptic first line is accessing the database in SEAMM (`_system_db`) and getting the name of the current *system* and *configuration*, which the **Reaction Step** ensures starts with “TS” if it is a transition state. The rest of the Python is self-explanatory. Unfortunately hard-wiring the symmetry number in this way makes the flowchart much less general, and is a temporary fix until the code can correctly determine the symmetry number from the structure.

We are almost done! The last part of the loop manipulates the energies that the **Structure** and **Thermochemistry** saved into variables, which can be accessed by any subsequent step, and then the two **Table** steps add a row to the table and store it as a comma

separated values (CSV) file to capture the key results in a convenient form for the user. Figure 6 shows the Custom step that transforms the computed energies and enthalpies into values relative to the reactants, and also captures the imaginary frequency of the transition states.

```

if _system_db.system.configuration.name == "reactants":
    Ereactants = energy
    ZPEreactants = ZPE
    Hreactants = H_thermal[0][0]
    Greactants = G_thermal[0][0]
    ZPE = round(ZPE, 2)
    E = round(energy - Ereactants, 2)
    H0 = round(E + ZPE - ZPEreactants, 2)
    H = round(E + H_thermal[0][0] - Hreactants, 2)
    G = round(E + G_thermal[0][0] - Greactants, 2)

transition_frequency = ""
if target == "transition state":
    n_imaginary = N_saddle_modes
    if n_imaginary == 1:
        transition_frequency = round(transition_state_frequency, 2)

```

Figure 6: The Python code handle the computed energies and enthalpies.

This is quite straightforward but shows the value of being able to customize the flowchart with a little bit of Python code. In this case, we are able to transform the energies into relative energies, which the next step adds to the table, as shown in Figure 7.

Append a row to		table	table1
Name	Value		
-	Structure	\$ _system_db.system.configuration.name	
-	E (kcal/mol)	\$E	
-	transition frequency (1/cm)	\$transition_frequency	
-	ZPE (kcal/mol)	\$ZPE	
-	H0 (kcal/mol)	\$H0	
-	H298 (kcal/mol)	\$H	
-	G298 (kcal/mol)	\$G	
+			

Figure 7: Adding a row of results to the table.

Note that the Table step is using the variables that were just defined in the Custom step

shown in Figure 6. This illustrates how the Python in `Custom` steps can access variables set by other steps, and how variables can be used in any of the fields in dialogs if preceded by a dollar sign ('\$') to indicate that it is a variable rather than a literal value. This ability to define and use variables, and insert small fragments of custom code, greatly enhance the capabilities of SEAMM and its flowcharts.

Reaction path for the Rearrangement of Methylisocyanide to Isonitrile

This flowchart, with the appropriate subflowchart in the `Structure`, `Reaction Path`, and `Thermochemistry` steps, was used successfully with a number of *ab initio* and semiempirical Hartree-Fock and density functional theory (DFT) methods, as reported in the article and shown there in Table 2. These calculations ran smoothly and only had minor problems, mainly due to the different default accuracies of the various methods. Loose convergence criteria for the energy and gradients caused the optimization of the structure of the transition state to fail to converge. The tightening of the convergence criteria for the energy and gradients resolved these issues.

The situation when using several different version of the ReaxFF forcefield⁸⁻¹⁰ and also different versions of the ANI parameterization of TorchANI^{11,12} was quite different. The NEB algorithm failed to converge or produced an unreasonable reaction path. For example, in some cases the nitrogen-carbon triple bond of the isonitrile broke, passing through a $\text{CH}_3\text{N} + \text{C}$ atom structure, with the carbon atom then inserting between the methyl group and nitrogen to form isocyanide. In other cases, the methyl-nitrogen bond broke to yield CH_3 and CN which then recombined to form the isonitrile. In yet other case, the structure exploded into separate atoms which then recombined to form the isonitrile. None of these paths is physically reasonable. We also noted that all of the forcefields and machine learning potentials predicted a bent structure for methylisocyanide, suggesting that the potentials

had fundamental issues reproducing the isocyanide group.

Unfortunately it is not easy to determine whether the training set for the forcefields or the machine learning potentials contained any isocyanides. Each of the forcefields used in this study were created by modifying existing forcefields to add new species and reactions. This required tracking the history of each forcefield and examining a number of papers and their supplementary information to understand the training set. As far as we can tell, none of the three ReaxFF forcefields examined contained an isocyanide in their training sets, but it is difficult to be certain.

The supplementary material associated with the ANI machine learning potentials contain the training sets used, which were subsets of the structures in available databases such as the GDB.¹³ Although GDB was produced by an exhaustive generation of plausible structures containing up to, for example, 11 atoms of C, N, O, and F, and hence contains structures with isocyanide functional groups, the selection of a subset does not guarantee that the training set for the ANI potentials contains any isocyanides. The supplementary material, though complete, is only machine readable, so it requires writing a small program to access the data to determine the molecules in the training set and find that there are no isocyanides included. Having access to the training data makes it possible to definitively determine whether specific functional groups, such as isocyanide, were included in the training; however, the need to write a program to access the data is a considerable barrier.

Focusing on the methylisocyanide structure, we can see that all the forcefields and ML potentials examined cannot describe the structure well. As noted above, all methods predict a bent structure rather than the linear structure observed experimentally. In addition, the calculated vibrational frequencies, shown in Table 1

Clearly, some of these frequencies are nonphysical and in general the differences between the calculated and experimental frequencies strongly suggest that neither the ReaxFF forcefields nor the ANI ML potentials can reasonably describe methylisocyanide, let alone the transition state.

Table 1: The vibrational frequencies (cm^{-1}) calculated for methylisocyanide.

Exptl. ^a	ReaxFF ¹⁴	ReaxFF ¹⁰	ReaxFF ⁸	ANI-1x ¹⁵	ANI-1cxx ¹⁶	ANI-2x ¹⁷
263	66	11	68	431	222	258
263	288	488	394	981	850	835
945	485	1304	946	1394	1304	1145
1129	1293	1333	960	1532	1521	1172
1129	1294	1352	1367	1757	1698	1445
1419	1949	1832	1475	2019	2026	1918
1467	2075	1889	1475	2031	2045	1990
1467	2075	1894	2942	2155	2109	2921
2166	3309	2074	3104	3241	3233	4266
2966	3388	3253	3105	4258	4221	4459
3014	3388	3254	3237	4354	4243	4581
3014	6952	3320	9016	4391	4280	4980

^a The experimental fundamental frequencies as quoted in Ref. 14.

References

- (1) Jónsson, H.; Mills, G.; Jacobsen, K. W. *Classical and Quantum Dynamics in Condensed Phase Simulations*; pp 385–404.
- (2) Henkelman, G.; Jónsson, H. Improved tangent estimate in the nudged elastic band method for finding minimum energy paths and saddle points. *The Journal of Chemical Physics* **2000**, *113*, 9978–9985.
- (3) Makri, S.; Ortner, C.; Kermode, J. R. A preconditioning scheme for minimum energy path finding methods. *The Journal of Chemical Physics* **2019**, *150*, 094109.
- (4) Smidstrup, S.; Pedersen, A.; Stokbro, K.; Jónsson, H. Improved initial guess for minimum energy path calculations. *The Journal of Chemical Physics* **2014**, *140*, 214106.
- (5) Henkelman, G.; Uberuaga, B. P.; Jónsson, H. A climbing image nudged elastic band method for finding saddle points and minimum energy paths. *The Journal of Chemical Physics* **2000**, *113*, 9901–9904.

- (6) Wang, L.-P.; Song, C. Geometry optimization made simple with translation and rotation coordinates. *The Journal of Chemical Physics* **2016**, *144*, 214108.
- (7) Larsen, A. H. et al. The atomic simulation environment—a Python library for working with atoms. *Journal of Physics: Condensed Matter* **2017**, *29*, 273002.
- (8) Strachan, A.; van Duin, A. C. T.; Chakraborty, D.; Dasgupta, S.; Goddard, W. A. Shock Waves in High-Energy Materials: The Initial Chemical Events in Nitramine RDX. *Phys. Rev. Lett.* **2003**, *91*, 098301.
- (9) Singh, S. K.; Srinivasan, S. G.; Neek-Amal, M.; Costamagna, S.; van Duin, A. C. T.; Peeters, F. M. Thermal properties of fluorinated graphene. *Phys. Rev. B* **2013**, *87*, 104114.
- (10) Shan, T.-R.; Wixom, R. R.; Thompson, A. P. *Nanoscale Void-Enhanced Initiation in Hexanitrostilbene: Reactive Molecular Dynamics Simulations.*; 2014.
- (11) Smith, J. S.; Nebgen, B. T.; Zubatyuk, R.; Lubbers, N.; Devereux, C.; Barros, K.; Tretiak, S.; Isayev, O.; Roitberg, A. E. Approaching coupled cluster accuracy with a general-purpose neural network potential through transfer learning. *Nature Communications* **2019**, *10*, 2903.
- (12) Devereux, C.; Smith, J. S.; Huddleston, K. K.; Barros, K.; Zubatyuk, R.; Isayev, O.; Roitberg, A. E. Extending the Applicability of the ANI Deep Learning Molecular Potential to Sulfur and Halogens. *Journal of Chemical Theory and Computation* **2020**, *16*, 4192–4202, PMID: 32543858.
- (13) Fink, T.; Reymond, J.-L. Virtual Exploration of the Chemical Universe up to 11 Atoms of C, N, O, F: Assembly of 26.4 Million Structures (110.9 Million Stereoisomers) and Analysis for New Ring Systems, Stereochemistry, Physicochemical Properties, Compound Classes, and Drug Discovery. *Journal of Chemical Information and Modeling* **2007**, *47*, 342 – 353.

- (14) Nguyen, T. L.; Thorpe, J. H.; Bross, D. H.; Ruscic, B.; Stanton, J. F. Unimolecular Reaction of Methyl Isocyanide to Acetonitrile: A High-Level Theoretical Study. *The Journal of Physical Chemistry Letters* **2018**, *9*, 2532–2538, PMID: 29697985.
- (15) Smith, J. S.; Nebgen, B.; Lubbers, N.; Isayev, O.; Roitberg, A. E. Less is more: Sampling chemical space with active learning. *The Journal of Chemical Physics* **2018**, *148*, 241733.
- (16) Smith, J. S.; Nebgen, B. T.; Zubatyuk, R.; Lubbers, N.; Devereux, C.; Barros, K.; Tretiak, S.; Isayev, O.; Roitberg, A. E. Approaching coupled cluster accuracy with a general-purpose neural network potential through transfer learning. *Nature Communications* **2019**, *10*, 2903.
- (17) Devereux, C.; Smith, J. S.; Huddleston, K. K.; Barros, K.; Zubatyuk, R.; Isayev, O.; Roitberg, A. E. Extending the Applicability of the ANI Deep Learning Molecular Potential to Sulfur and Halogens. *Journal of Chemical Theory and Computation* **2020**, *16*, 4192–4202, PMID: 32543858.